XV. COMMUNICATIONS BIOPHYSICS*

Academic and Research Staff

Prof. S. K. Burns
Prof. L. S. Frishkopf
Prof. J. L. Goldstein†
Prof. J. J. Guinan, Jr.†
Prof. R. W. Henry‡
Prof. P. G. Katona
Prof. W. T. Peake†
Prof. W. A. Rosenblith
Prof. W. M. Siebert
Prof. T. F. Weiss**†
Prof. M. L. Wiederhold†
Dr. J. S. Barlow††
N. I. Durlach
Dr. R. D. Hall
Dr. P. L. Hill
Dr. N. Y. S. Kiang†
Dr. R. W. Lansing‡‡
R. M. Brown†
A. H. Crist†
W. F. Kelley
L. H. Seifel

Graduate Students

T. Baer
J. E. Berliner
L. D. Braida
H. S. Colburn
P. Demko, Jr.
G. M. Goldmark
Z. Hasan
A. J. M. Houtsma
D. H. Johnson
D. W. Kress, Jr.
A. F. Krummenoehl
E. C. Moxon
W. M. Rabinowitz
A. V. Reed
D. O. Stahl II
R. S. Stephenson
A. P. Tripp, Jr.
D. R. Wolfe

Undergraduate Students

D. R. Dutton
J. S. Gishen
Sharon Grundfest
G. R. Ladd
R. A. McPherson
W. L. Nuffer
S. C. Poppe
R. E. Reder
E. A. Soykota
J. P. Yu

A. ON STOCHASTIC NEURAL MODELS OF THE DIFFUSION TYPE

One common simple model for the stochastic behavior of neurons is shown in Fig. XV-1. Excitatory and inhibitory synaptic inputs are represented by positive and negative impulse trains, respectively. The effects of temporal and spatial integration are modelled by the action of a linear time-invariant system with impulse response

$$h(t) = \begin{cases} e^{-\alpha t}, & t > 0 \\ 0, & t < 0. \end{cases}$$

---

*This work was supported principally by the National Institutes of Health (Grant 5 PO1 GM14940-03), and in part by the Joint Services Electronics Programs (U.S. Army, U.S. Navy, and U.S. Air Force) under Contract DA 28-043-AMC-02536(E), and the National Aeronautics and Space Administration (Grant NGL 22-009-304).

†Also at the Eaton-Peabody Laboratory, Massachusetts Eye and Ear Infirmary, Boston, Massachusetts.

‡Visiting Associate Professor from the Department of Physics, Union College, Schenectady, New York.

**Research Associate in Preventive Medicine, Harvard Medical School, Boston, Massachusetts.

††Research Affiliate in Communication Sciences from the Neurophysiological Laboratory of the Neurology Service of the Massachusetts General Hospital, Boston, Massachusetts.

‡‡Postdoctoral Fellow from the Department of Psychology, University of Arizona, Tucson, Arizona.

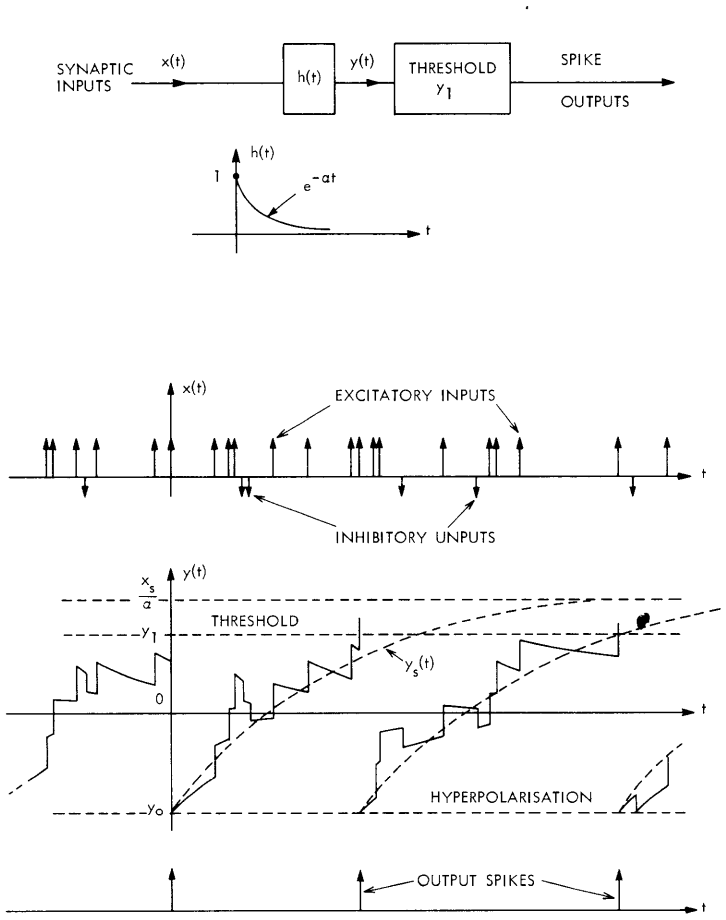

Fig. XV-1. Model for the stochastic behavior of neurons.

All postsynaptic potentials (PSP) are thus assumed to have the same exponential shape (although perhaps different amplitudes) with the same time constant. The output y(t) of the integrator is usually interpreted as the membrane potential of the postsynaptic neuron at the point of spike initiation. Immediately following a spike [It is convenient to take this moment as the time origin. Many authors include an absolutely refractory period, but analytically this is a trivial modification that we shall ignore.] the membrane potential is reset to some hyperpolarized value $y_o < 0$ from which it would decay exponentially to a resting value (taken as zero) in the absence of any synaptic input. Synaptic inputs, however, cause the membrane potential to follow another course; if in its wanderings it intersects the threshold value, y_1, then another spike is initiated.

Models more or less of this kind have been proposed and studied by many workers.[1-9] Interest has centered primarily on the statistics of the interspike intervals when the inputs are random (Poisson) impulse trains. Most of these studies have been concerned with simulations, since a complete analytical solution to the problem appears to be possible[3] only if $\alpha = 0$ (no decay of the PSP). Formulas for the moments

of the interspike interval distribution have been given[8] for $a \neq 0$ if the amplitude of each PSP is very small compared with threshold, but no closed-form representations for the interval distribution have been published for even a special combination of parameters if $a \neq 0$. The purpose of this report is to describe one such special case in which an explicit formula for the interval distribution can in fact be derived.

We shall assume, in common with many of the studies referenced above, that each PSP is sufficiently small and that the (constant) average rate at which they occur is sufficiently high that the random component $x_n(t)$ of the input to the integrator for $t > 0$ is effectively gated stationary white noise with autocorrelation function $\sigma^2 u_o(\tau)$ (where $u_o(\tau)$ is a unit impulse). We shall also assume that the input contains a steady, constant, nonrandom component of amplitude x_s representing the average imbalance of excitatory and inhibitory inputs (or, perhaps, some other effective input such as has been postulated to explain pacemaker action[10]). Since the integrator is linear, its output can be considered as the sum of two components; a noise term $y_n(t)$, which is a Gaussian random process with zero mean and autocorrelation function $E[y_n(t)y_n(\tau)] = R_n(t, \tau) = \frac{\sigma^2}{2a}\left[e^{-a(t-\tau)} - e^{-a(t+\tau)}\right]$; $0 < t, \tau$ ($y_n(t)$ is nonstationary because the integrator is assumed to be reset to y_o at $t = 0$), and a nonrandom term

$$y_s(t) = \frac{x_s}{a} + \left(y_o - \frac{x_s}{a}\right) e^{-at}, \qquad t > 0.$$

The noise term, $y_n(t)$, is a particular example of a Markov diffusion process, and has been much studied under the name of the Ornstein-Uhlenbeck process.[11]

Qualitative arguments suggest (and simulations have proved) that the character of the interspike interval distribution depends markedly on the relationship between the threshold, y_1, and the final value, x_s/a, of $y_1(t)$. For x_s/a substantially less than y_1, the interval distribution is highly asymmetric with an exponential "tail," whereas for x_s/a significantly larger than y_1, the interval distribution is more nearly symmetric and "Gaussian" in appearance. The intermediate case, $x_s/a \approx y_1$, is harder to visualize and the resulting distribution, being intermediate, is harder to describe. But, remarkably, for $x_s/a = y_1$ an analytical solution for the interval distribution can be obtained in terms of elementary functions, as we now show.

The key to the derivation is an extension of the reflection principle of André[12] to the Ornstein-Uhlenbeck process. Let $M(t, k)$ be the event $y_n(\tau) = k\, e^{-a\tau}$ for some τ in the range $0 \leq \tau \leq t$. Then it is more or less immediately obvious that for any number, d,

$$P[y_n(t) \geq d \,|\, M(t, k)] = P\left[y_n(t) \leq 2k\, e^{-at} - d \,\middle|\, M(t, k)\right].$$

The argument depends upon the fact that if at any time, say $t = t_1$, we know the value of $y_n(t)$, then $y_n(t)$ for $t \geq t_1$ may be considered as the sum of two components: one is

$y_n(t_1)\, e^{-\alpha(t-t_1)}$, and the other is a noise process whose distribution at any time $t \geq t_1$ is symmetric about zero.

To apply this principle to the problem at hand, let $d = k\, e^{-\alpha t}$ and multiply both sides by $P[M(t,k)]$ to obtain

$$P\left[y_n(t) \geq k\, e^{-\alpha t}, M(t,k)\right] = P\left[y_n(t) \leq k\, e^{-\alpha t}, M(t,k)\right].$$

But of course, if $y_n(t) \geq k\, e^{-\alpha t}$ (we assume henceforth that $k \geq 0$), then $M(t,k)$ must have occurred so that

$$P\left[y_n(t) \geq k\, e^{-\alpha t}, M(t,k)\right] = P\left[y_n(t) > k\, e^{-\alpha t}\right]$$

$$= \frac{1}{\sqrt{2\pi}} \int_{k\, e^{-\alpha t}}^{\infty} \frac{1}{\sqrt{R_n(t,t)}} \exp\left(-\frac{y^2}{2R_n(t,t)}\, dy\right).$$

Now let $\overline{M}(t,k)$ be the complement of the event $M(t,k)$. Then the union of the compound event $y_n(t) \leq k\, e^{-\alpha t}$ and $M(t,k)$ with the disjoint compound event $y_n(t) \leq k\, e^{-\alpha t}$ and $\overline{M}(t,k)$ is just the event $y_n(t) \leq k\, e^{-\alpha t}$. Hence

$$P\left[y_n(t) \leq k\, e^{-\alpha t}, M(t,k)\right] + P\left[y_n(t) \leq k\, e^{-\alpha t}, \overline{M}(t,k)\right]$$

$$= P\left[y_n(t) \leq k\, e^{-\alpha t}\right]$$

$$= \frac{1}{\sqrt{2\pi}} \int_{-\infty}^{k\, e^{-\alpha t}} \frac{1}{\sqrt{R_n(t,t)}} \exp\left(-\frac{y^2}{2R_n(t,t)}\, dy\right).$$

Moreover, since $\overline{M}(t,k)$ includes the event $y_n(t) \leq k\, e^{-\alpha t}$,

$$P\left[y_n(t) \leq k\, e^{-\alpha t}, \overline{M}(t,k)\right] = P[\overline{M}(t,k)].$$

Finally, combining yields

$$P[\overline{M}(t,k)] = \sqrt{\frac{2}{\pi}} \int_{0}^{k\, e^{-\alpha t}} \frac{1}{\sqrt{R_n(t,t)}} \exp\left(-\frac{y^2}{2R_n(t,t)}\, dy\right).$$

To apply this formula to our problem, observe that the probability that $y_n(\tau)$ does <u>not</u> cross through $(y_1 - y_o)\, e^{-\alpha\tau}$ in $0 \leq \tau \leq t$ is identical with the probability that

$y_n(\tau) + \frac{x_s}{a} + \left(y_o - \frac{x_s}{a}\right) e^{-a\tau}$ does not cross through y_1 in $0 \leq \tau \leq t$, if $y_1 = x_s/a$. If p(t) is the density distribution for the first passage time (i.e., the interspike interval distribution), then

$$\int_t^\infty p(\tau)\, d\tau = P[\bar{M}(t, y_1 - y_o)]$$

or

$$p(t) = -\frac{\partial}{\partial t}\{P[\bar{M}(t, y_1 - y_o)]\}$$

$$= \frac{2(y_1 - y_o)\, a^{3/2}}{\sqrt{\pi}\,\sigma} \frac{e^{2at}}{(e^{2at} - 1)^{3/2}} \exp\left[-\frac{(y_1 - y_o)^2\, a}{\sigma^2 (e^{2at} - 1)}\right]; \qquad t > 0$$

which is our final result.

In the limit $a \to 0$, we readily obtain

$$\lim_{a \to 0} p(t) = \frac{(y_1 - y_o)}{\sqrt{2\pi}\,\sigma t^{3/2}} \exp\left[-\frac{(y_1 - y_o)^2}{2\sigma^2 t}\right]; \qquad t > 0$$

which is the well-known[3, 13] result for the distribution of the first passage times of a zero-drift Wiener process through a threshold (or absorbing barrier) at $(y_1 - y_o)$. For $a = 0$, the moments of the interspike interval distribution are all ∞, because the "tail" vanishes only as $t^{3/2}$. For $a \neq 0$, however, the "tail" of the interval distribution vanishes exponentially and all of the moments are finite. In fact, it is elementary, if algebraically tedious, to show that

$$E(t) = \int_0^\infty t p(t)\, dt = \int_0^\infty P[\bar{M}(t, y_1 - y_o)]\, dt$$

$$= \frac{1}{a} \int_0^{(y_1 - y_o)\frac{\sqrt{2a}}{\sigma}} e^{u^2/2} \left[\int_u^\infty e^{-v^2/2}\, dv\right] du$$

which is a formula that has been previously given[8, 14] for the mean of the interval distribution in this case.

The shape of p(t) is shown in Figs. XV-2 and XV-3 for various values of $\gamma = \frac{(y_1 - y_o)\sqrt{a}}{\sigma}$ on both linear and semi-logarithmic scales. Some of the more obvious features follow.

1. For any value of γ, p(t) is unimodal with an exponential "tail"; indeed it is easy to show analytically that

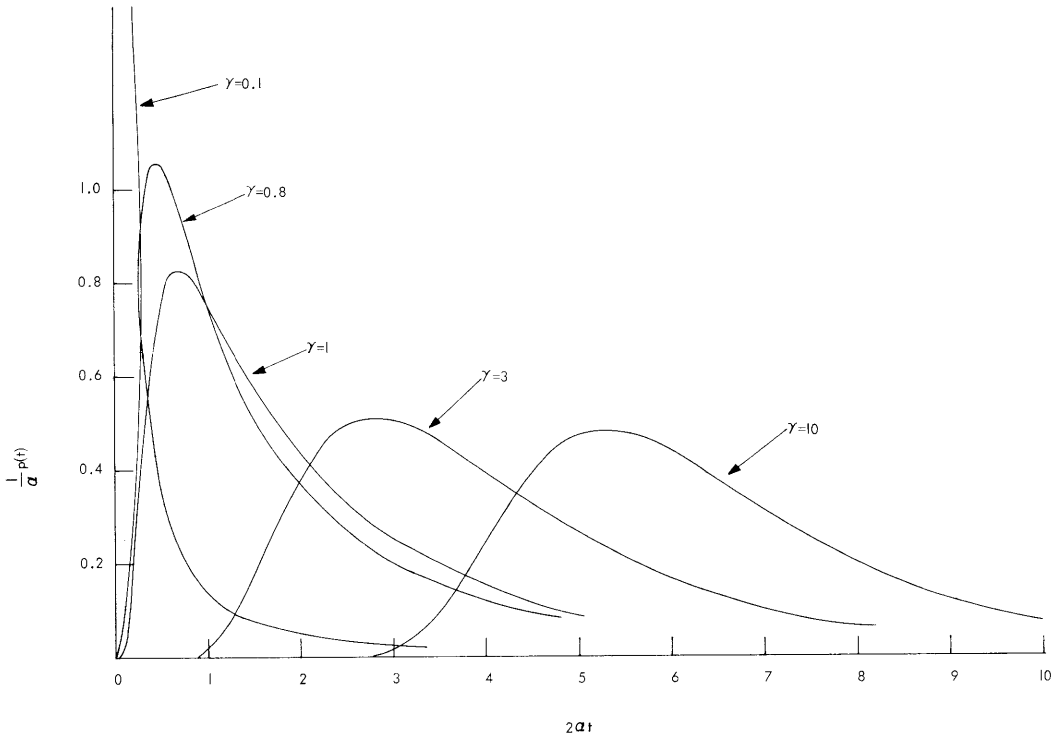

Fig. XV-2. Interval histograms.

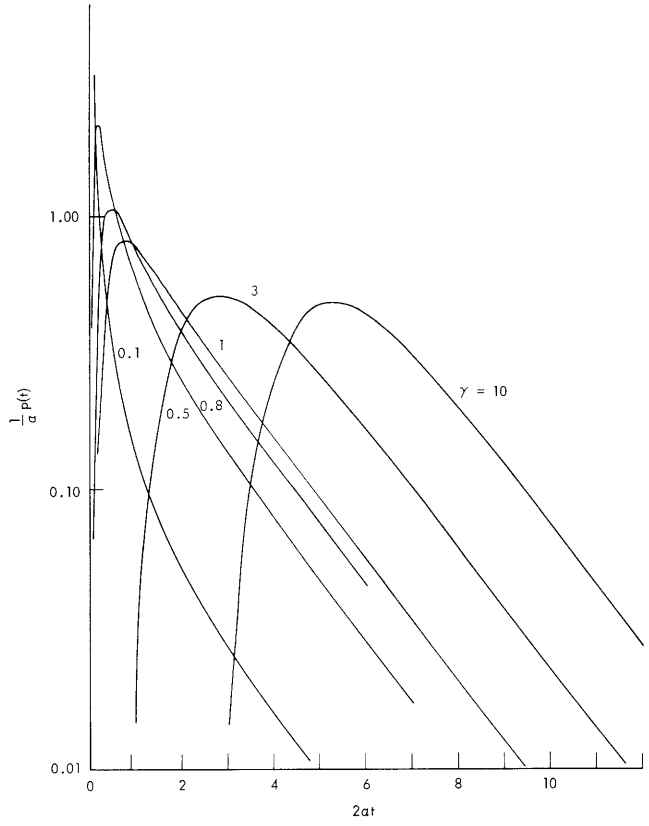

Fig. XV-3. Interval histograms.

$$p(t) \rightarrow \frac{2a\gamma}{\sqrt{\pi}} e^{-at}$$

as $t \rightarrow \infty$.

2. For small values of $\gamma \ll 1$ (i.e., noise large), p(t) is highly skewed and has a concave-upward "tail" on a semi-logarithmic plot that has been often described as "slower than exponential" or "nonexponential" behavior. For large values of $\gamma \gg 1$, p(t) is more nearly symmetric.

Physiological histograms with similar shapes have often been observed.[3]

W. M. Siebert

References

1. G. L. Gerstein, "Mathematical Models for the All-or-None Activity of Some Neurons," IRE Trans., Vol. IT-8, pp. 137-143, 1962.
2. E. E. Fetz and G. L. Gerstein, "An RC Model for Spontaneous Activity of Single Neurons," Quarterly Progress Report No. 71, Research Laboratory of Electronics, M.I.T., October 15, 1963, pp. 249-257.
3. G. L. Gerstein and B. Mandelbrot, "Random Walk Models for the Spike Activity of a Single Neuron," Biophys. J. 4, 41-68 (1964).
4. C. F. Stevens, Letter to the Editor, Biophys. J. 4, 417-419 (1964).
5. B. Gluss, "A Model for Neuron Firings with Exponential Decay of Potential Resulting in Diffusion Equations for Probability Density," Bull. Math. Biophys. 29, 233-243 (1967).
6. R. B. Stein, "A Theoretical Analysis of Neuronal Variability," Biophys. J. 5, 173-194 (1965).
7. R. B. Stein, "Some Models of Neuronal Variability," Biophys. J. 7, 37-68 (1967).
8. P. I. M. Johannesma, "Diffusion Models for the Stochastic Activity of Neurons," in Neural Networks, E. R. Caianiello (ed.) (Springer-Verlag, New York, 1968), pp. 116-144.
9. J. P. Segundo, D. H. Perkel, H. Wyman, H. Hegstad, and G. P. Moore, "Input-Output Relations in Computer-Simulated Nerve Cells," Kybernetik 4, 157-171 (1968).
10. D. Junge and G. P. Moore, "Interspike-Interval Fluctuations in Aplysia Pacemaker Neurons," Biophys. J. 6, 411-434 (1966).
11. D. R. Cox and H. D. Miller, The Theory of Stochastic Processes (John Wiley and Sons, Inc., New York, 1965), pp. 226 ff.
12. A. Papoulis, Probability, Random Variables and Stochastic Processes (McGraw-Hill Book Company, Inc., New York, 1965), p. 505.
13. D. R. Cox and H. D. Miller, op. cit., p. 221.
14. Ibid., p. 249.

B. CONTROL OF A SENSORY-MOTOR REFLEX IN CRAYFISH

A preliminary report[1] described a situation in crayfish abdomen in which what appears to be a monosynaptic sensory-motor reflex arc is regulated by sensory input of different modality. The basic reflex arc comprises the negative feedback system diagrammed in Fig. XV-4 for the n^{th} abdominal segment. Passive flex of segment n+1 relative to segment n causes an elongation of the tonic receptor muscle and an increase in spike frequency on the stretch receptor (SR) neuron. The sensory input causes spikes on a motor neuron, and the resulting tension in superficial extensor muscle fibers tends to oppose the original flexion.

The branch of the second root which includes the SR neuron runs between the superficial extensor muscles and the dorsal exoskeleton, and a pin or wire electrode inserted through the shell can pick up SR spikes and summed junction potentials from many fibers

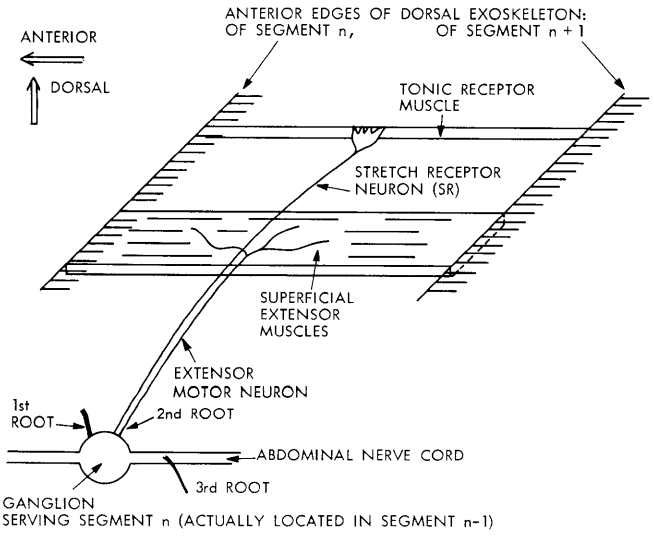

Fig. XV-4. Diagram of the relations between nerves and muscles involved in the basic sensory-motor reflex.

of these muscles. The reflex is seen as a muscle junction potential beginning ~20 msec after an SR spike. We call such a muscle junction potential a time-locked muscle (TLM) wave. The synapse (or synapses) involved in this reflex must lie in the ganglion serving that segment because the TLM waves persist when the central nerve cord is cut anterior and/or posterior to that ganglion.

The fraction of SR spikes that are followed by TLM waves varies from 0 to nearly 1. Presumably, this variation is caused by inputs to the motor neuron either from other sensory neurons or from the CNS. In particular, we found[2] that sensory input produced

by the disturbance of hairs on the exoskeleton can increase the fraction of SR spikes followed by TLM waves from a typical spontaneous value of 0.1 or less to as high as 0.9.

We thought originally that the hairs responsible for the enhancing effect on the reflex were quite widespread, but later experiments with small electrically driven probes have shown that most, if not all, of the hairs involved lie on the posterior edge of a segment where they are moved by relative movement between that segment and the next posterior one. Though input from hairs on several segments can increase the TLM/SR fraction in a given segment, we still cannot put numbers on the relative enhancement from different segments because of our present inability to monitor the stimulus strength. (We can find afferent "touch" neurons – also in the second root – which fire in response to movement of the hairs, but we have not yet been able to tell whether only one or more than one afferent fiber produces the regulatory effect.)

Since one of the reasons for our work is to look for plastic properties of synapses,

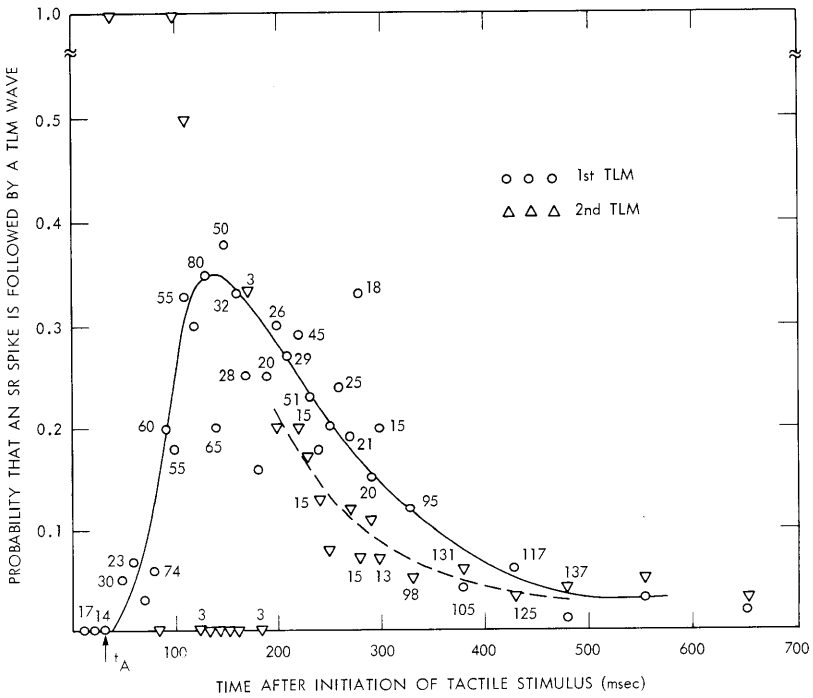

Fig. XV-5. Probability that an SR spike is followed by a TLM wave vs time of TLM wave measured from initiation of tactile stimulus. A burst of tactile nerve spikes begins at time t_A. Solid curve (circles): only SR spikes preceding the first TLM wave after the stimulus are counted. Dashed curve (inverted triangles): only SR spikes occurring between first and second TLM waves after the stimulus are counted. Numbers next to data points represent the number of SR spikes used in the calculation of that probability. Time window: 10 msec for $0 < t \leq 300$ msec, and 50 msec for $t > 300$ msec.

we have attempted to quantify the regulatory effect of the "touch" input on the SR-muscle reflex. In a typical experiment we recorded SR spikes and TLM waves while several hundred mechanical stimuli, in the form of short puffs of air, were directed at an area of exoskeleton on segment 3 at intervals of approximately 1 sec, while the SR neuron in segment 3 was firing at approximately 10 spikes/sec. We plotted two PST (post-stimulus-time) histograms: (a) of the first TLM wave following the stimulus, and (b) of all stretch receptor spikes (delayed by 20 msec) occurring between the stimulus and the first TLM wave. The ratio of histogram (a) to histogram (b) is a PST histogram of the probability that an SR spike at time t-20 msec is followed by a TLM wave at time t. This probability (shown by the circles and the solid curve in Fig. XV-5) rises to a maximum in ~100 msec and decays in another 300 msec. The burst of afferent spikes on "touch" neurons in response to the air puff can be recorded. It begins at time t_A (shown on the graph in Fig. XV-5) and seems to last no more than ~30 msec. The data also show that the occurrence of a TLM seems to "reset" the synapse to some degree. That is, the probability that an SR spike that occurs after the first TLM wave elicits a second TLM wave at time t is always lower than the corresponding probability for the first TLM wave at time t. The PST probability for the second TLM wave is shown by the inverted triangles and dashed curve in Fig. XV-5.

These results suggest a model in which a short burst of spikes on a "touch" neuron momentarily increases the sensitivity of the synapse(s) between the SR neuron and the extensor motor neuron. Many facets of this regulatory effect remain to be studied: for example, its dependence on number of spikes in a "touch" burst, on SR firing rate, and on segment of origin of the "touch" input, the additivity of inputs from different segments, whether the effect habituates, and the isolation of other sources of control of the basic reflex.

R. W. Henry, Z. Hasan

References

1. S. Chang, "Tactile Gating of a Crayfish Stretch Receptor Reflex," S. B. Thesis, M. I. T., June 1968.

2. Z. Hasan, "Neural Control of a Proprioceptive Reflex in Crayfish," S. M. Thesis, M. I. T., January 1969.

C. AUDITORY MASKING

The masked threshold (the level of masker just needed to reduce detection of the signal in a two-interval, two-alternative forced-choice experiment to 75% correct) was measured when the masker was rectangular narrow-band (10 Hz wide) Gaussian noise and the signal was a pure tone of fixed frequency. The variable parameters were the signal intensity and the center frequency of the noise. The masker was generated in accordance with the following representation: $n(t) = x_c(t) \cos 2\pi f_m t - x_s(t) \sin 2\pi f_m t$, where $x_c(t)$ and $x_s(t)$ are independent, lowpass Gaussian processes with identical spectra. The spectrum of n(t) was "clean" 55 dB below the level of the narrow band of noise centered at f_m, and its edges cut off at the rate of 5 dB/Hz.

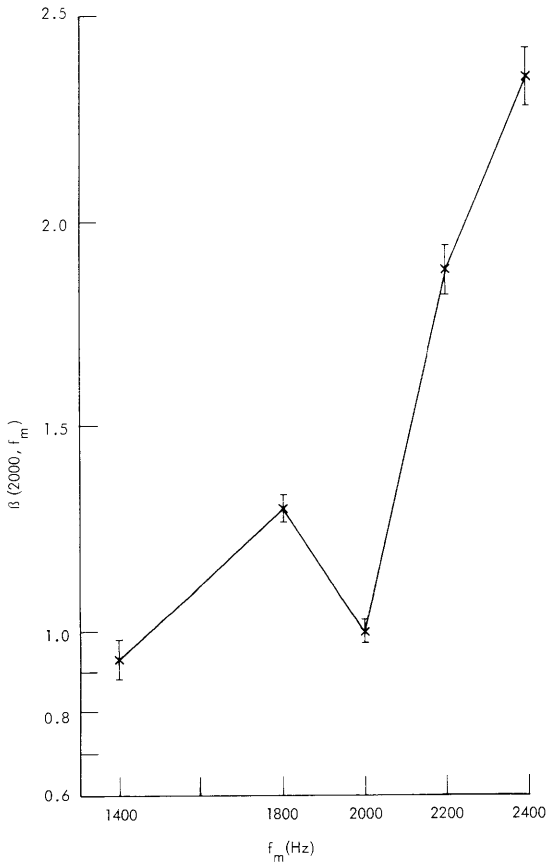

Fig. XV-6.
Slope of the incremental masking function vs f_m for f_s = 2000 Hz. Vertical bars indicate estimated standard deviation for 200 trials. Subject: P. G.

The incremental masking function (the change in the masked threshold for a given change in the signal intensity) was found to be adequately described by a power law over the 20-dB range of signal intensities used in our experiment. That is,

$$\left(\frac{I_{mt1}}{I_{mt2}}\right) = \left(\frac{I_{s1}}{I_{s2}}\right)^{\beta(f_s, f_m)},$$

where I_{mt1} is the masked threshold corresponding to I_{s1}, and so forth. Figure XV-6 gives the exponent, $\beta(f_s, f_m)$, for a signal frequency of 2000 Hz for one subject. The exponent was found to be almost always greater than or equal to one; it was found to be greater than one for masker center frequencies just below and above the signal frequency, while it was precisely one when the masker was at the signal frequency. The exponents for maskers tested below and above the signal frequency increase monotonically with increasing masker frequency. Figure XV-7 shows psychophysical tuning curves constructed from the same data. Earlier experimenters did not characterize their masking functions by a power law, nor did they find a decreased effectiveness of the

masker at higher intensities for $f_m < f_s$. It is suggested that distortion in their equipment was responsible for these differences.

A physiological explanation of these results was sought in terms of the excitatory and

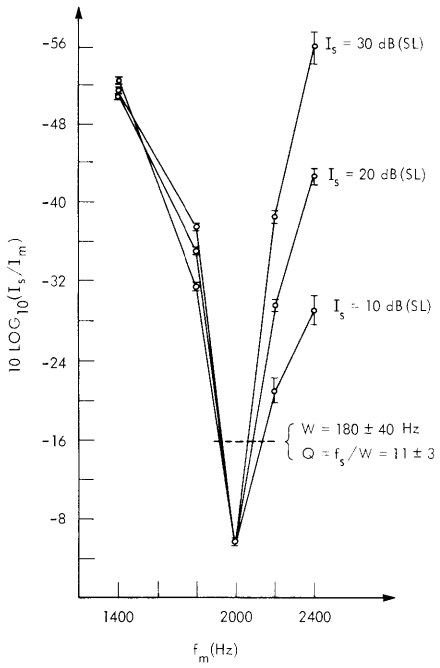

Fig. XV-7.
Psychophysical tuning curves. f_s = 2000 Hz. Subject: P.G.

inhibitory responses that are known to occur in the auditory nerve.[1,2] By using the description of two-tone inhibition formulated by M. B. Sachs,[2] an approximation to the neural discharge function, and by assuming a constant rate-ratio threshold, a power law was predicted. The exponent of this power law bears a similar relation to stimulus parameters as the exponent found in the psychophysical masking experiment.[3]

D. O. Stahl II

References

1. M. B. Sachs and N. Y. S. Kiang, "Two-Tone Inhibition in Auditory-Nerve Fibers," J. Acoust. Soc. Am. 43, 1120-1128 (1968).
2. M. B. Sachs, "Stimulus-Response Relation for Auditory-Nerve Fibers: Two-Tone Stimuli," J. Acoust. Soc. Am. 45, 1025-1035 (1969).
3. D. O. Stahl II, "Psychophysical Tuning Curves," S.M. Thesis, M.I.T., June 1969.

D. MICROELECTRODE RECORDINGS OF INTRACOCHLEAR POTENTIALS

[These results were presented at the 77th Meeting of the Acoustical Society of America, April 10, 1969. Abstract published in the Program of the 77th Meeting, p. 36.]

A variety of electric potentials have been recorded from the cochlea during the last 40 years, but relatively little is known about how these potentials are generated, and their role in the signal transmission processes of the ear is a subject of much speculation. In our experiments we recorded electric potentials from micropipettes as they were advanced through the cochlear partition of cats' ears that were stimulated by tones. Following the electrophysiological experiments the cochleae were examined histologically to determine how closely the recording of electrical events might be associated with specific cochlear structures.

1. Methods

Our experimental apparatus is illustrated in Fig. XV-8. Micropipettes (with tip diameters probably in the range of a few micrometers to a few tenths of a micrometer, filled with 2MKCl) were advanced with a hydraulic system through the round-window membrane into the cochlear partition in the extreme basal end of the cochlea. On an inkwriter oscillograph we recorded as follows.

1. The position of the electrode drive as obtained from a potentiometer on the micrometer movement.

2. The DC potential recorded by the moving electrode referred to an electrode on the chin of the cat.

3. The amplitude of the response recorded by stationary electrodes: either a gross electrode near the round window, and/or a micropipette in a cochlear scala.

4. The magnitude of the impedance of the moving electrode at 25 Hz. This measurement was made by injecting a 25-Hz current through the electrode and measuring the amplitude of the 25-Hz voltage as detected through a bandpass filter. Usually this impedance is purely resistive at 25 Hz, although the reactive component can be significant at higher frequencies in the audio range.

5. and 6. The amplitude and phase of the fundamental component of the response to the tone recorded by the moving electrode as detected through a narrow-band (2 Hz) electrically tuned filter.

In addition to the oscillograph record of the variables as functions of time, an x-y plotter displayed DC potential vs electrode position. Other combinations of variables could be plotted, since the data were recorded on magnetic tape.

The electrode holder (Fig. XV-9) was attached to a hydraulic system. At the

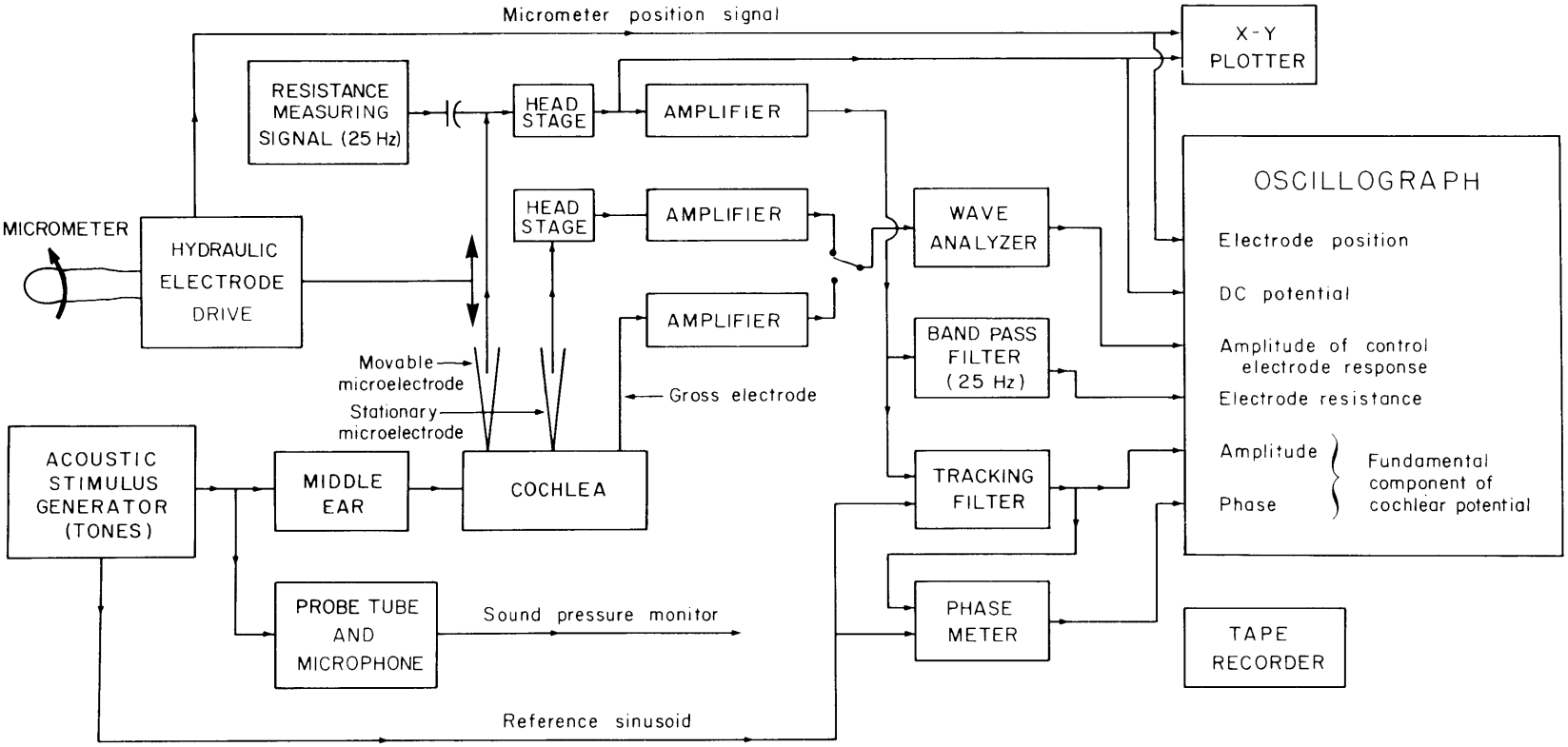

Fig. XV-8. Schematic of the experimental apparatus.

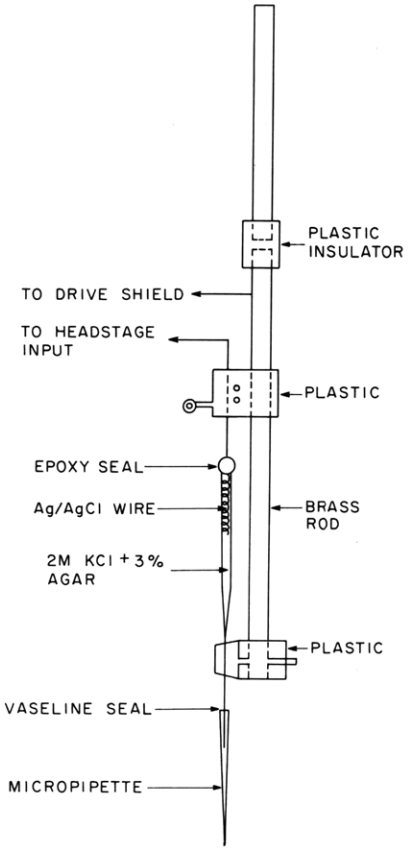

Fig. XV-9. Sketch of the electrode holder.

completion of a traverse of the cochlea, cement was poured into the bulla cavity so as to cover the round window and surround the micropipette. The hydraulic system was used to withdraw the electrode holder, while the micropipette was held in the cochlea by the cement and separated from the rest of the assembly at the vaseline seal. The electrode remained in place in the temporal bone throughout fixation, decalcification, dehydration, and embedding in celloidin. For sectioning, the bone was oriented so that sections were taken in an approximately transverse plane that was almost parallel to the electrode. A deviation of the plane of section from the axis of the pipette was chosen so that the tip of the electrode was cut before the thicker stub. In some cases the electrode tip remained in the tissue. In other cases we could find other indications of the position of the electrode pass. We have been unsuccessful in locating electrode passes when the electrode was not left in the tissue during histological procedures.

2. Results

a. Correlation of Electrophysiology and Anatomy

Figure XV-10 shows an example of an oscillographic record obtained as the micropipette advanced through the organ of Corti. Many of our principal observations can be described by dividing the electrode pass into 5 regions (1 through 5 in Fig. XV-10).

In three regions (1, 3, and 5) the electrode resistance, DC and AC potentials are relatively constant for large displacements of the electrode. In agreement with the conclusions of many others (starting with von Békésy, in 1952, and Tasaki, Davis, and Eldredge, in 1954[1, 2]) we feel that these three regions are probably (i) scala tympani, (ii) scala media, and (iii) scala vestibuli. In the other two regions the electrode resistance and DC potential change rapidly, presumably as the electrode penetrates Reissner's membrane (4) and the basilar membrane and organ of Corti (2).

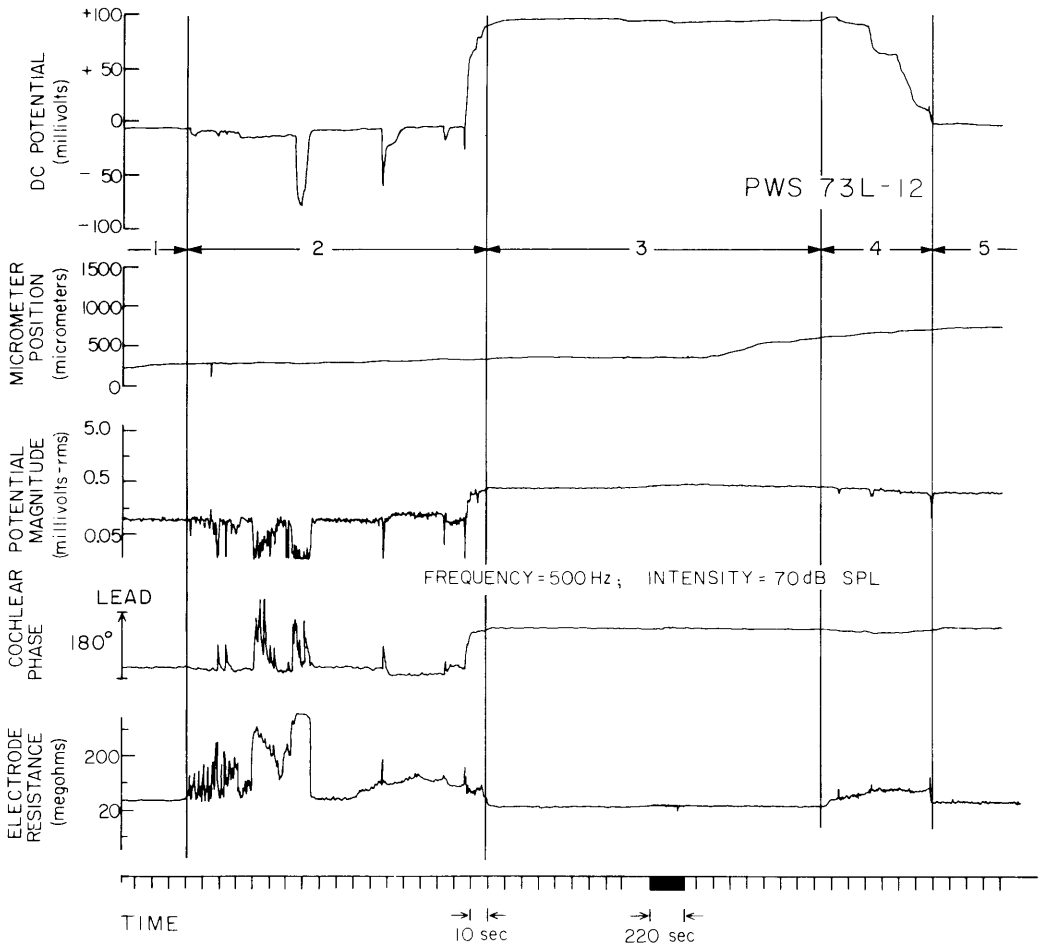

Fig. XV-10. An example of oscillographic records obtained when a micropipette is advanced through the organ of Corti. Regions 1 through 5 are thought to correspond to the intervals when the electrode is passing through (1) scala tympani, (2) organ of Corti, (3) scala media, (4) Reissner's membrane, (5) scala vestibuli.

Figure XV-11 shows some of these same variables plotted against electrode position. In agreement with von Békésy,[1] and Tasaki, Davis and Eldredge,[2] we find that the

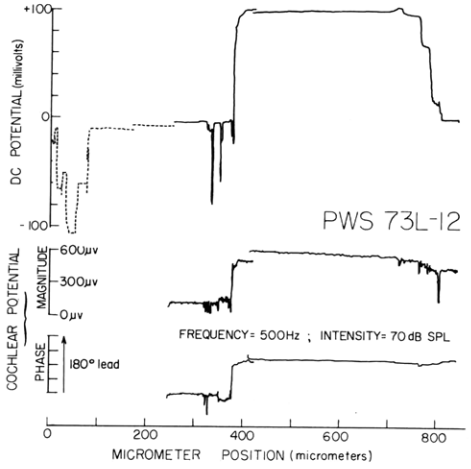

Fig. XV-11.

D-C potential and the amplitude and phase of the fundamental components of the cochlear potential vs electrode position. These plots were made from a magnetic tape. The break and overlap of the lines at the 400-μ position results from a period (1 1/2 hours) of recording responses to tones in this location. The vertical separations at this point represent changes in the recorded variables over this time. The horizontal overlap results from drift in the recording electronics. The dashed portion of the top record was recorded from an earlier penetration of the round window in the same location.

amplitude and phase of the cochlear potential change abruptly when the large positive DC potential is contacted. The characteristics of these changes will be discussed separately in the report following this one.

Figure XV-12 (left) shows a histological section containing an electrode tip. A close inspection of the section shows that the electrode passes through the tunnel of Corti. DC potential vs position is plotted on the right on the same scale. We can see that there is at least a rough correspondence (in this case) between the anatomical and physiological distances. We can make comparisons more easily in Fig. XV-13 where the same DC profile is superimposed on an outline tracing of the histological section. The distance traveled by the electrode from touching the round window to the region in which negative potentials are found is approximately equal to the distance across the scala tympani along the electrode track in the section. Also the region just before the positive potential is encountered is approximately the width of the organ of Corti; the distance over which the positive potential is nearly constant is approximately the same as the width of scala media. In this case an intermediate positive potential level was recorded which continues for some distance. Perhaps this can be associated with the distortion of Reissner's membrane that appears in the section.

Even this rough correspondence of anatomical and physiological distances does not always obtain. In Fig. XV-14 for instance, the distance over which the positive potential was held is approximately twice the width of scala media. The picture suggests that the electrode tip was in the bone before the positive potential disappeared! It is not possible in this case, and in many others, to arrange the DC profile and the anatomical section to give a reasonable correspondence of distances.

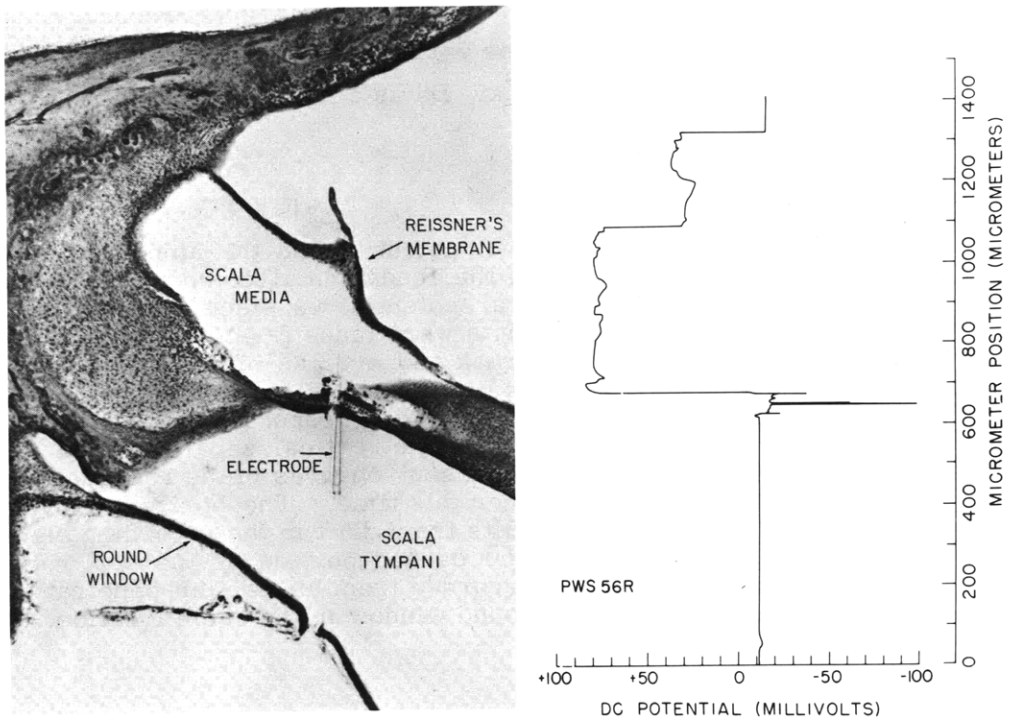

Fig. XV-12. Left: Photomicrograph of a 40-μ section through the cochlea containing the tip of the micropipette. Right: DC potential vs electrode position. The vertical scale in the right-hand plot is equal to the scale on the left, and the photomicrograph has been oriented so that the apparent direction of the electrode pass is vertical.

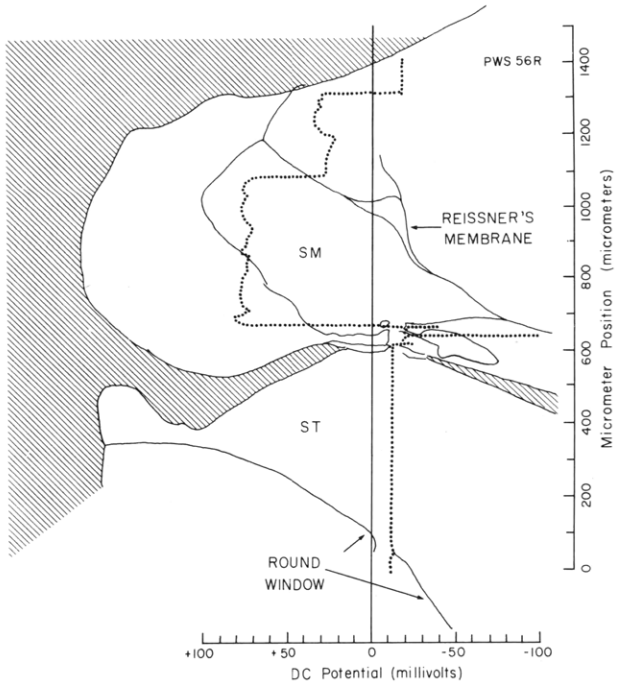

Fig. XV-13.

Overlay of the DC profile from the right of Fig. XV-12 on an outline drawing from the photomicrograph on the left.

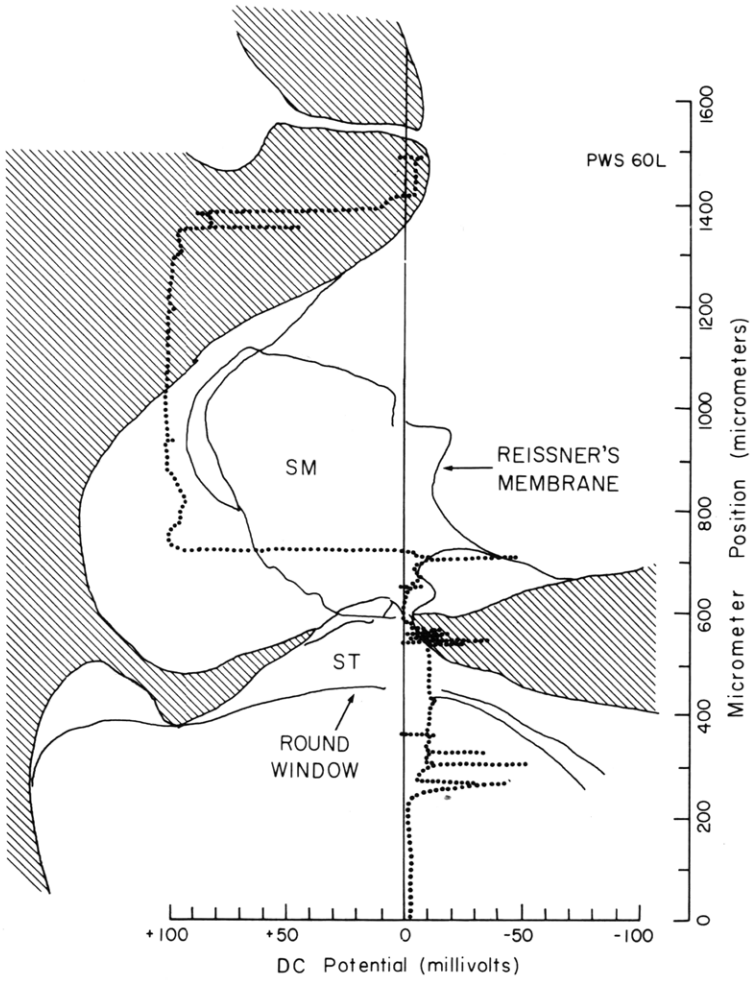

Fig. XV-14. A DC profile (dotted) superimposed on an outline of a photomicrograph containing a clear indication of the electrode track through the tunnel. No matter how the DC profile is moved up and down with respect to the histological section, it is difficult to associate the changes in potential with the structures.

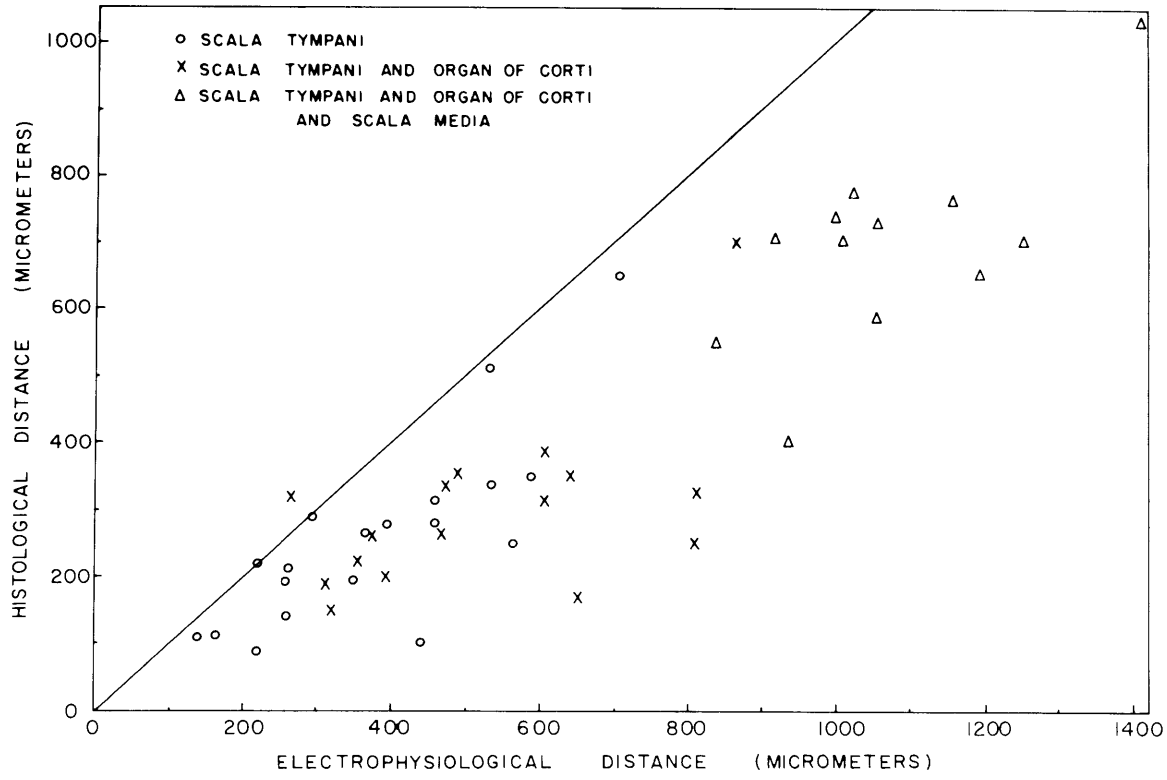

Fig. XV-15. Scatter plot of all measured histological distances from the sections along the electrode track. The electrophysiological distances were obtained from the DC profiles and correspond to the distances moved in region 1 (circles), 1 + 2 (x's), 1 + 2 + 3 (Δ's).

In Fig. XV-15 histological distance measurements are plotted against electrophysiological distances for a number of cochleae. Although the histological and electrophysiological distances are not uncorrelated, the large spread of the data suggests that it would not be possible to define the position of the electrode at any one time with enough precision to say whether it was in a particular cell.

Some indications of the variability in the physiological distance measurements are seen in Fig. XV-16, in which superimposed records of the DC potential were taken as the electrode was moved in and out, along the same path. We see that the physiological measurements of distance can vary considerably. For instance, the width of scala media as measured from the positive potential region in these records ranges from 350 μ to 700 μ. It is easy to think of other possible sources of discrepancies between the two distance measures – factors such as electrode bending and distortion of the histological material. We have not attempted to assess the relative importance of these factors. It seems clear that electric events that extended in space for distances of 10's of microns or less certainly cannot be associated with specific small anatomical structures by this technique.

3. D-C Potentials

Figure XV-17 is a histogram of the amplitude of the positive DC potential referred to scala tympani (endolymphatic potential). For the 51 cochleae included here, 88% have an endolymphatic potential between 90 mV and 115 mV. The average is ~100 mV.

Figure XV-18 is a histogram of the potential difference between scala tympani and scala vestibuli. Of the 38 values plotted here, 90% are within the range ±10 mV. The average is approximately 0 mV.

Measurements with intracochlear electrodes in guinea pigs (most recently and extensively by Lawrence[3] and Butler[4]) have indicated a large negative potential in the organ of Corti which can be recorded with electrodes having large (30-μ) tips[3] and over rather large distances.[4] This potential has been called the "Corti potential," and is presumed to exist in the large extracellular spaces of the organ of Corti. Our records do not show any potential with these characteristics. Figure XV-19 shows the general instability of DC potential, cochlear response amplitude, and electrode resistance that is encountered just before the advancing electrode contacts the large positive potential. (Incidentally, we see on the lower trace that the amplitude of the cochlear response from a stationary electrode in scala media does not change appreciably as the moving electrode passes through the organ of Corti.) In most penetrations we encounter a few negative potentials in this region – often as large as 100 mV. Usually the negative potential decreases rapidly and is gone within a few seconds, even if the electrode advance is stopped when the negative potential is encountered.

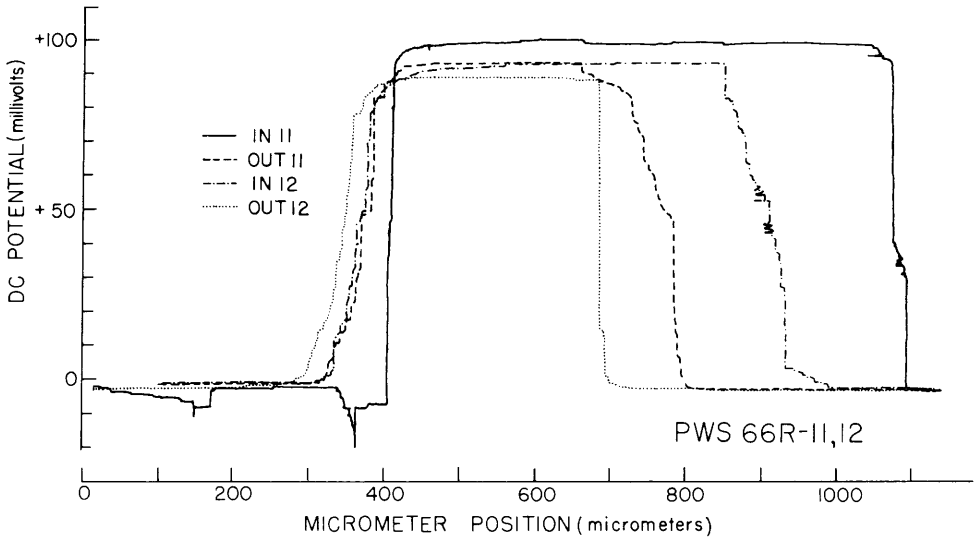

Fig. XV-16. D-C profiles for four traverses through the organ of Corti along the same path.

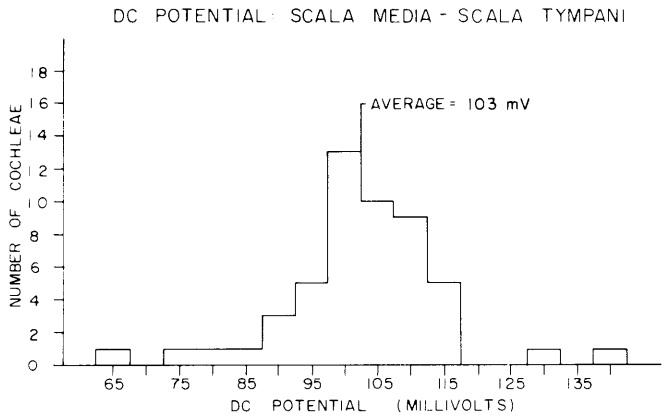

Fig. XV-17.

Histogram of endolymphatic potential determined from measurements of the first penetration of micropipettes into 51 cochleae.

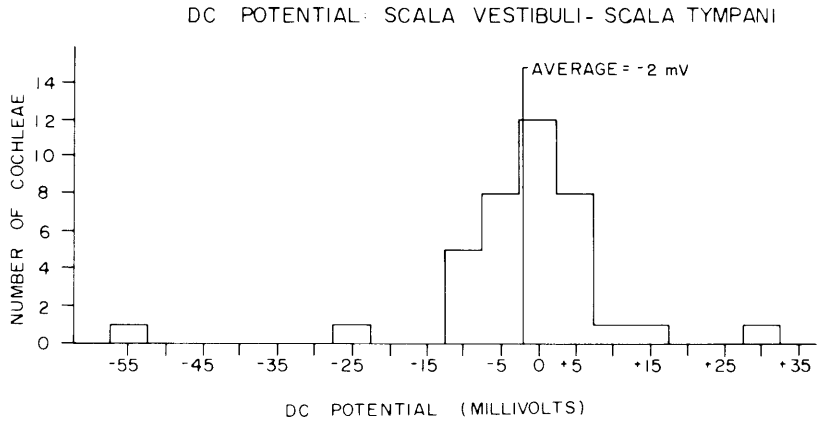

Fig. XV-18. Histogram of DC potential between scala tympani and scala vestibuli (38 cochleae).

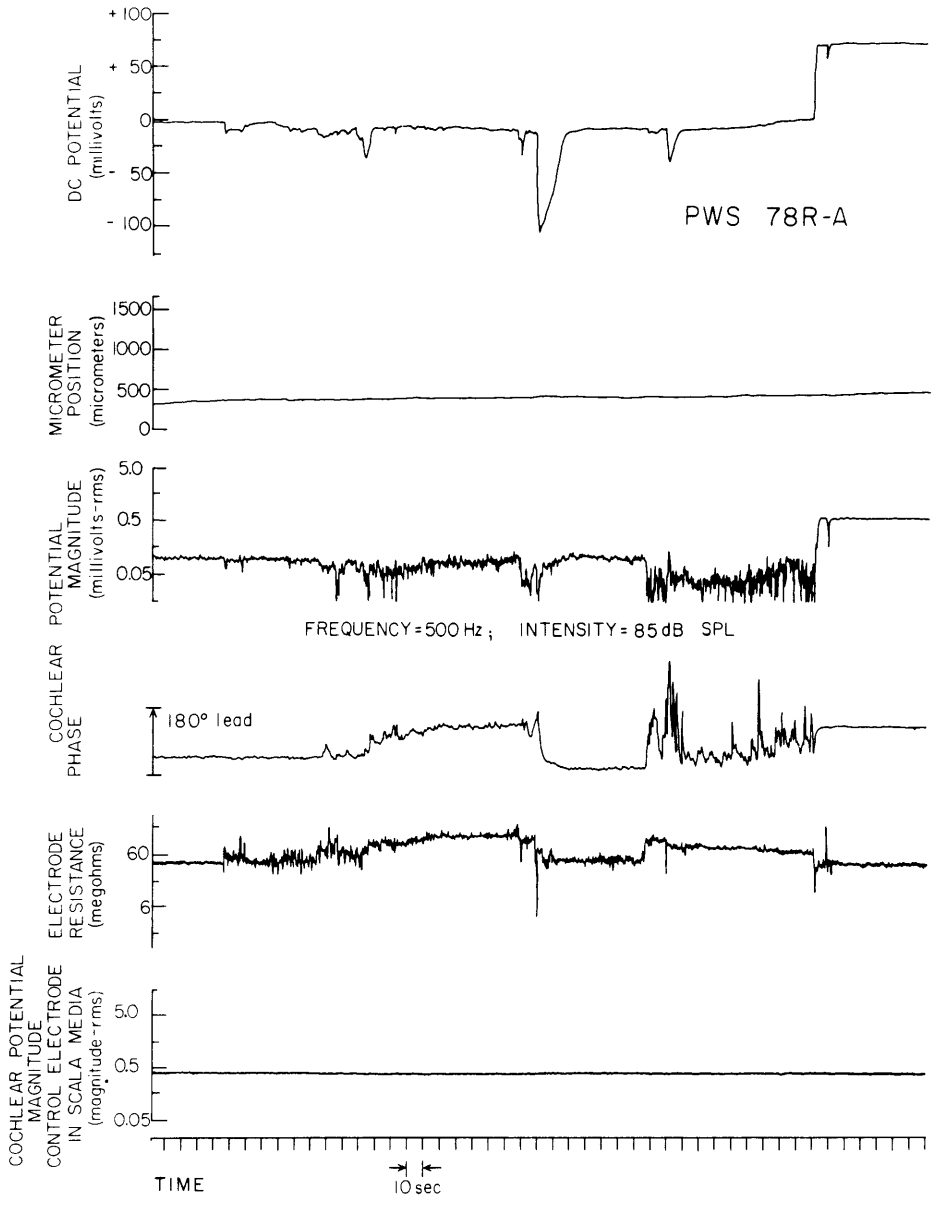

Fig. XV-19. Oscillograph records obtained just before the moving electrode contacted the positive potential. The lower trace was recorded from a micropipette that had been advanced into scala media before these records were taken.

DC potential vs position is shown in Fig. XV-20 for another penetration. The negative deflections just to the right of the positive potential region are typical of our results, in that negative potentials greater than 10 mV or 20 mV are not maintained for more than a few micrometers of electrode movement. Hence we do not record a potential having properties that one might expect for an extracellular "Corti potential." We feel quite sure from our histological results that some of our penetrations have passed through the hair-cell region. Some must have gone through the spaces of Nuel and the tunnel – large extracellular spaces. In none of these passes have we encountered a negative DC potential of the size obtained by Butler and Lawrence in the guinea pig (that is, from -40 mV to -100 mV) which were maintained over distances of tens of microns. Figure XV-20

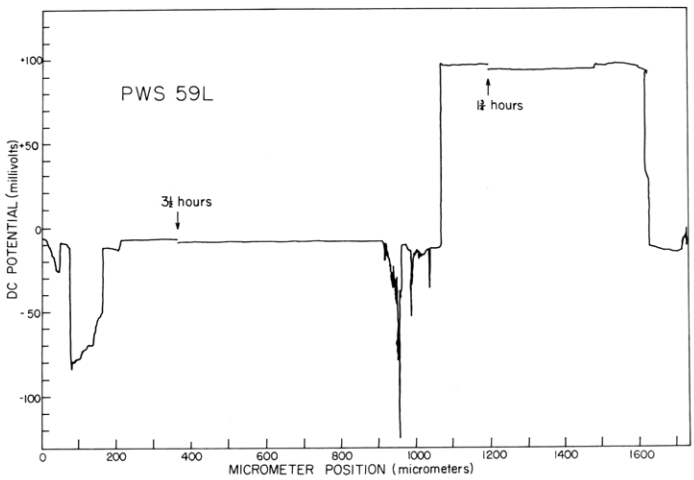

Fig. XV-20. D-C profile for a penetration in which the left-hand negative deflections probably occurred as the electrode went through the round-window membrane.

shows at the left a fairly unusual record of a large negative potential that was held over approximately 100 μ. Probably the electrode tip was in the round-window membrane here.

Since we have not been able to obtain large negative potentials in the organ of Corti that are maintained for large electrode displacements, we have not determined the conditions necessary for recording this result, and we cannot really settle this issue. We should point out that although Lawrence[3] displays DC potential vs position in plots similar to some of ours, there are important differences in our techniques. When we encountered a large change in potential, we stopped moving the electrode. In most of Lawrence's records the electrode is advanced at a constant speed of 5 μ/sec. This difference in procedure can clearly make a large difference in the appearance of the curves.

W. T. Peake, H. S. Sohmer, T. F. Weiss

(Harvey S. Sohmer is now associated with the Department of Physiology, Hadassah Medical School, Hebrew University, Jerusalem.)

References

1. G. von Békésy, "D-C Resting Potentials inside the Cochlear Partition," J. Acoust. Soc. Am. 24, 72-76 (1952).
2. I. Tasaki, H. Davis, and D. H. Eldredge, "Exploration of Cochlear Potentials in Guinea Pig with a Microelectrode," J. Acoust. Soc. Am. 26, 765-773 (1954).
3. M. Lawrence, "Electrical Polarization of the Tectorial Membrane," Ann. Otol. Rhinol. Laryngol. 76, 287-313 (1967).
4. R. A. Butler, "Some Experimental Observations on the dc Resting Potentials in the Guinea Pig Cochlea," J. Acoust. Soc. Am. 37, 429-433 (1965).

E. INTRACOCHLEAR RESPONSES TO TONES

[These results were presented at the 77th Meeting of the Acoustical Society of America, April 10, 1969. Abstract published in the Program of the 77th Meeting, p. 36.]

During penetrations of the cochlea with microelectrodes (described in Sec. XV-D) we obtained data on cochlear potentials in response to tones in the scalae of the basal turn of the cat's cochlea.

Our principle results are summarized as follows.

1. Relatively large changes in cochlear potentials are found across the organ of Corti; that is, between scala tympani and scala media. The changes in both the magnitude and phase of cochlear potentials are dependent on stimulus level and frequency. Relatively small changes in cochlear potentials are found across Reissner's membrane and during the traverse of a scala.

2. To a first-order approximation the magnitude of the cochlear potentials recorded from the basal turn appears to be proportional to the magnitude of the stapes velocity. Data of von Békésy appear to be consistent with this result.

1. Methods

Our conclusions are based on data obtained from 31 cat cochleae. In two of these cochleae the auditory nerve had been cut two weeks before the experiment.

In the last 18 cochleae in the series a swept-tone technique (illustrated in Fig. XV-21) was used. An oscillator mechanically locked to a level recorder was swept in frequency. The oscillator drove a condenser earphone housed in a probe tube assembly that was inserted into the external auditory meatus. A calibrated probe tube was used to measure the pressure near the eardrum. The output of the probe tube was amplified and fed to a tracking filter. The tracking filter had a 2-Hz bandwidth centered on the frequency of the oscillator. The magnitude of the ouput of the tracking filter could be plotted directly on the level recorder as a continuous function of frequency. The output

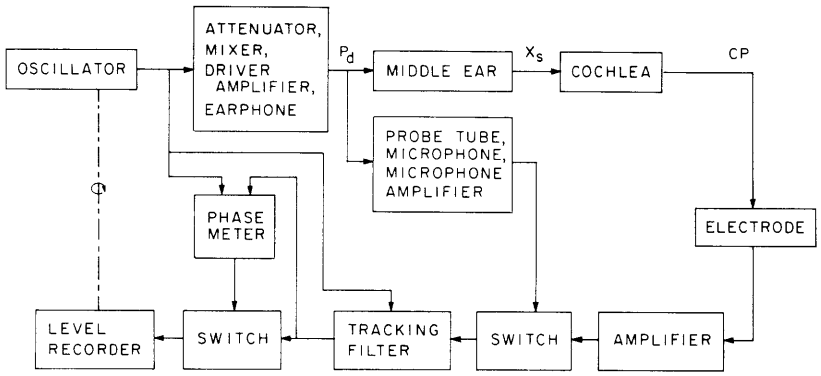

Fig. XV-21. Diagram of the system used to record responses to swept tones. P_d is the drum pressure, X_s is the stapes displacement, and CP is the cochlear potential in response to tones. Cochlear potentials were measured with respect to a reference electrode placed in an incision on the cat's chin.

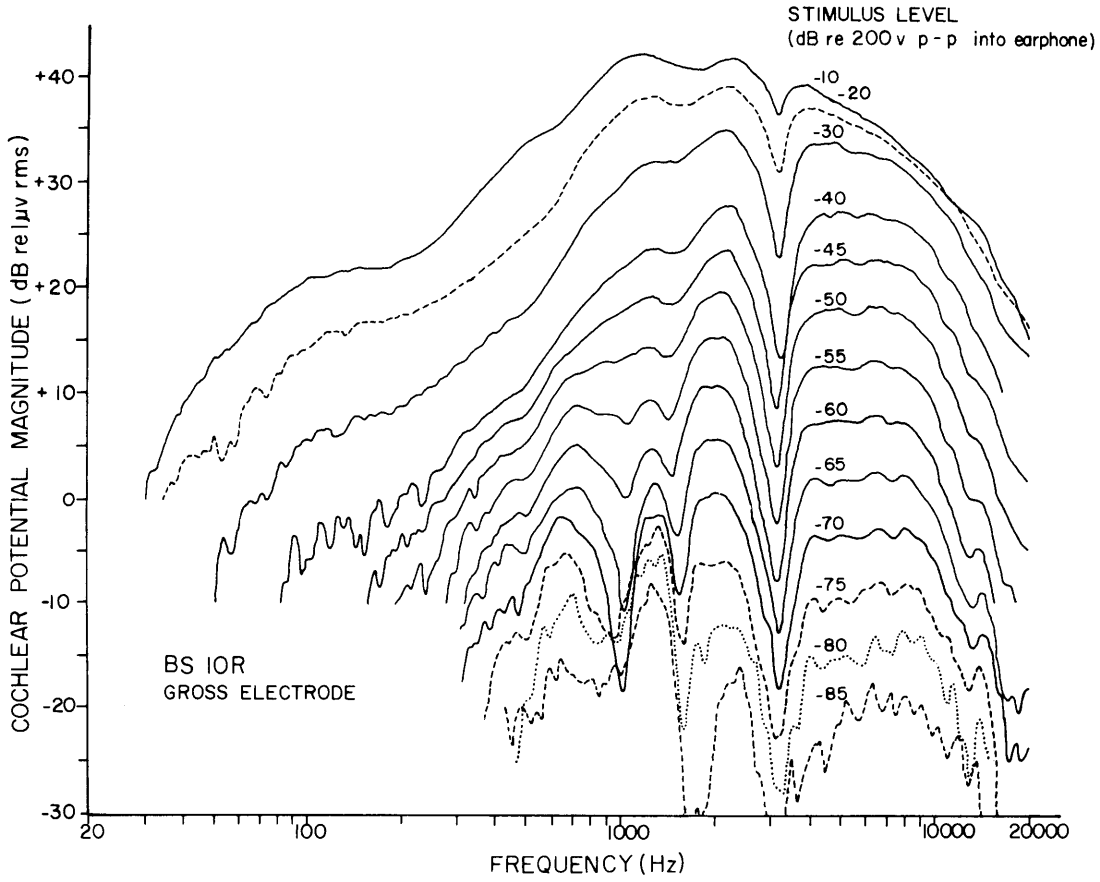

Fig. XV-22. Magnitude of the fundamental component of the cochlear potential in response to tones as a function of frequency. These data were obtained from a gross electrode on the surface of the cochlea. In this particular case the bony septum between the middle-ear cavity and the bulla cavity was intact, which accounts for the level-independent dip around 3.5 kHz.[10]

of the tracking filter also went to a phase meter whose output could also be plotted as a continuous function of frequency. Potentials recorded with intracochlear microelectrodes could be analyzed in the same way as indicated in Fig. XV-21. Thus the results to be presented are based upon the magnitude and phase of the fundamental of the response to a tone.

The magnitude of the cochlear potential obtained from an electrode located on the surface of the cochlea is shown in Fig. XV-22. Data with a similar format were obtained with intracochlear microelectrodes.

The same swept-tone techniques were used in all calibration procedures, as well as in measuring the impedances of microelectrodes in situ. The latter measurements were used to indicate in an approximate manner the maximum frequency below which the measurements were probably not significantly affected by the frequency characteristics of the microelectrode and headstage system.

2. Results

a. Changes in Intracochlear Potential as a Function of Electrode Position

The ratio of the magnitudes of cochlear potentials in scala media to scala vestibuli, that is, across Reissner's membrane, are shown in Fig. XV-23. Data from 4 animals at one stimulus level are shown as a function of frequency. Except for the data obtained from PWS84L at frequencies above 1 kHz the curves deviate from 0 dB by no more than +8 dB over more than 2 decades of frequency. This ratio does not depend strongly on stimulus level.

In Fig. XV-24 it is shown that the phase shift of cochlear potentials between scala media and scala vestibuli is relatively small and not strongly dependent on stimulus frequency. Other data indicate that this phase shift is not strongly dependent on stimulus level. We conclude, therefore, that cochlear potentials are larger in scala media than in scala vestibuli by perhaps as much as a factor of two, and the potentials are approximately in phase in these two scalae.

In contrast to these results, large changes in cochlear potential occur when an electrode is advanced from scala tympani to scala media. As indicated in Fig. XV-25, the magnitude of the ratio of cochlear potentials in scala media to scala tympani can be larger than 20 dB. Although the data vary considerably from cat to cat, the tendency appears to be for this ratio to be large at low frequencies and to decrease toward 0 dB at 2-3 kHz. Above 2-3 kHz a trend is less clearly discernible. The spread in the data at high frequencies may be due partly to differences in frequency responses of microelectrodes in the different experiments. The data shown were obtained with the same voltage level into the earphone, but not necessarily for the same drum pressure for each

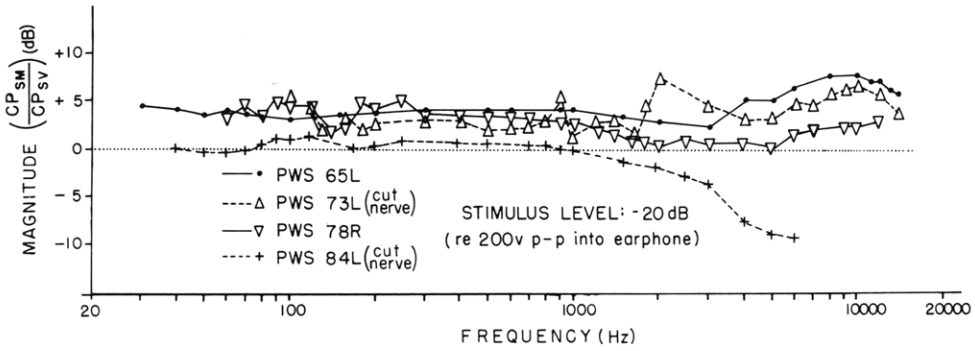

Fig. XV-23. Ratio of magnitudes of cochlear potentials across Reissner's membrane (CP_{SM}/CP_{SV}) vs frequency for 4 cochleae. Solid lines correspond to data obtained from normal cochleae. Dashed lines correspond to data obtained from cochleae whose auditory nerve had been severed.

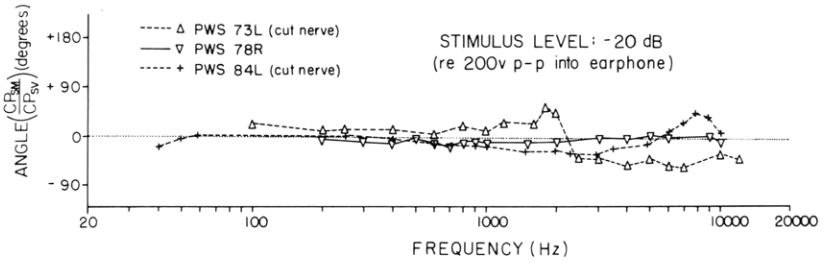

Fig. XV-24. Phase shift of cochlear potentials across Reissner's membrane (scala media minus scala vestibuli) vs frequency for 3 cochleae. Solid lines correspond to data obtained from a normal cochlea. Dashed lines correspond to data obtained from cochleae whose auditory nerve had been severed.

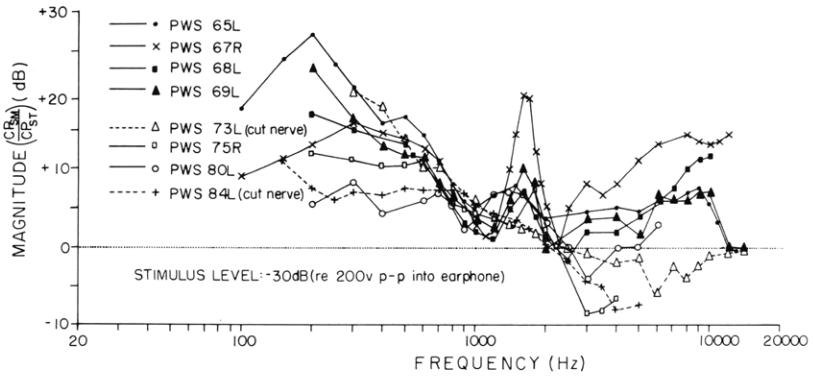

Fig. XV-25. Ratio of magnitudes of cochlear potentials across the organ of Corti (CP_{SM}/CP_{ST}) vs frequency for 8 cochleae. Solid lines correspond to data obtained from normal cochleae. Dashed lines correspond to data obtained from cochleae whose auditory nerve had been severed.

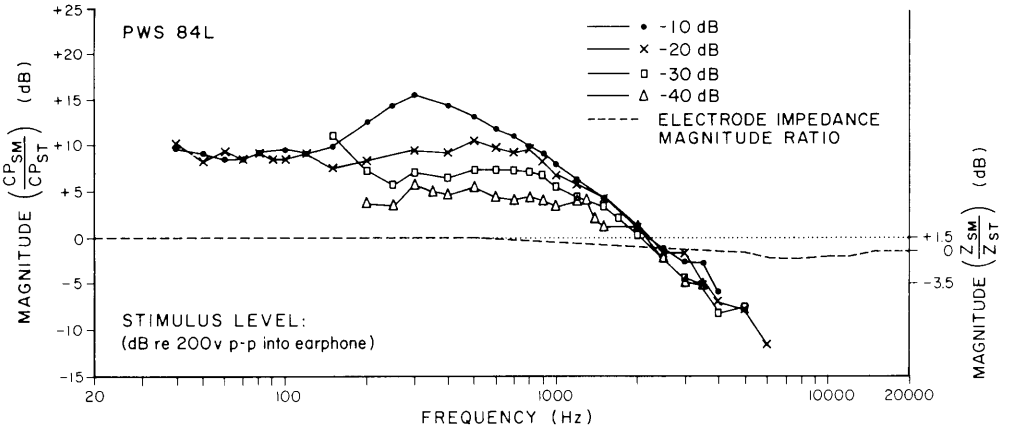

Fig. XV-26. Ratio of magnitudes of cochlear potentials across the organ of Corti (CP_{SM}/CP_{ST}) vs frequency for one cochlea (solid lines). The parameter is stimulus level. Dashed line is the ratio of magnitudes of the microelectrode impedances in scala media to scala tympani (Z_{SM}/Z_{ST}). The auditory nerve to this cochlea was severed.

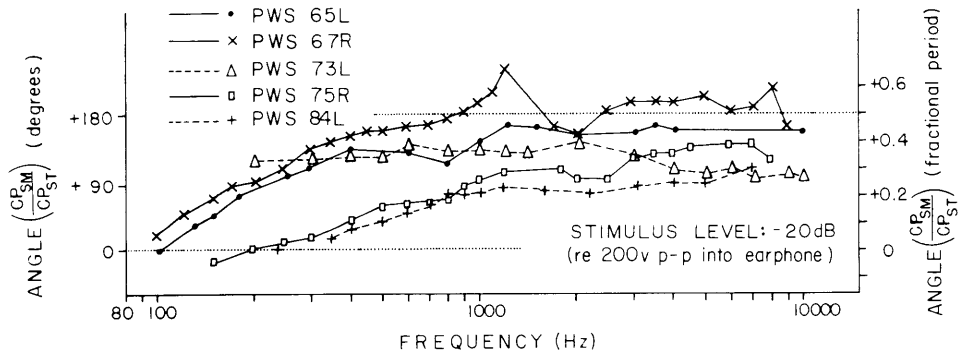

Fig. XV-27. Phase difference of cochlear potentials (scala media minus scala tympani) vs frequency. Solid lines correspond to data obtained from normal cochleae. Dashed lines correspond to data obtained from animals whose auditory nerve had been severed.

animal. These differences may account in part for the variations in the results from animal to animal. Between 1 kHz and 2 kHz there appears to be a peak in the data for the normal animals. The two cut-nerve animals do not show this peak. Other observations lead us to conclude that this effect is due primarily to the neural component of the response.

In Fig. XV-26 it is shown that the ratio of cochlear potentials in scala media to scala tympani depends on stimulus level, as well as on stimulus frequency. Even though the data across animals show considerable variation, the level dependence of this function shows consistent trends for any one animal, as is illustrated in Fig. XV-26. The ratio of cochlear potential in scala media to scala tympani is larger at high levels for almost all frequencies.

The difference in phase between cochlear potentials in scala media and scala tympani for 5 different cochleae at the same stimulus voltage level is shown in Fig. XV-27. These curves seem to approach zero at low frequencies and head toward values ranging from 90° to 180° at high frequencies. This phase shift is also level-dependent.

From such data we conclude that during a traverse of the cochlea, the largest changes in cochlear potentials are seen across the organ of Corti. Relatively small changes are seen across Reissner's membrane and during the traverse of a single scala. Between scala tympani and scala media, the phase difference of cochlear potentials is usually less than 180°. Since a phase difference of 180° has been both widely reported[1-8] and assumed to be consistent with the hypothesis that the sources of cochlear potential in response to sound are contained within the organ of Corti, it might be useful to try to interpret this result by examining a relatively simple network model of the distribution of AC potentials in the cochlea.

Two adjacent incremental portions of a one-dimensional distributed-network model of the cochlea are shown in Fig. XV-28. Each scala is assumed to be an equipotential at a longitudinal position x cm from the stapes, with the potentials of scalae vestibuli, media, and tympani shown as the top three nodes in the circuit. The reference node at the bottom represents the body of the animal. The voltage-current characteristic of all cross-sectional boundaries of the scalae are represented by admittances per unit length (the Y's), except for the boundary between scala tympani and scala media. No assumption is made about this boundary, except that it can be represented as a two-terminal device. This assumption implies, however, that no current is assumed to flow in the longitudinal direction within the organ of Corti. Adjoining incremental portions of the cochlea are assumed to be coupled resistively through the lymphs. This coupling is represented by the small r's, which are resistances per unit length of the scalae.

The following conclusions can be derived from this network,[9] subject to the restriction that the spatial distribution of cochlear potentials in response to tones is broad compared with the spread of potential attributable to a point source in the cochlea.

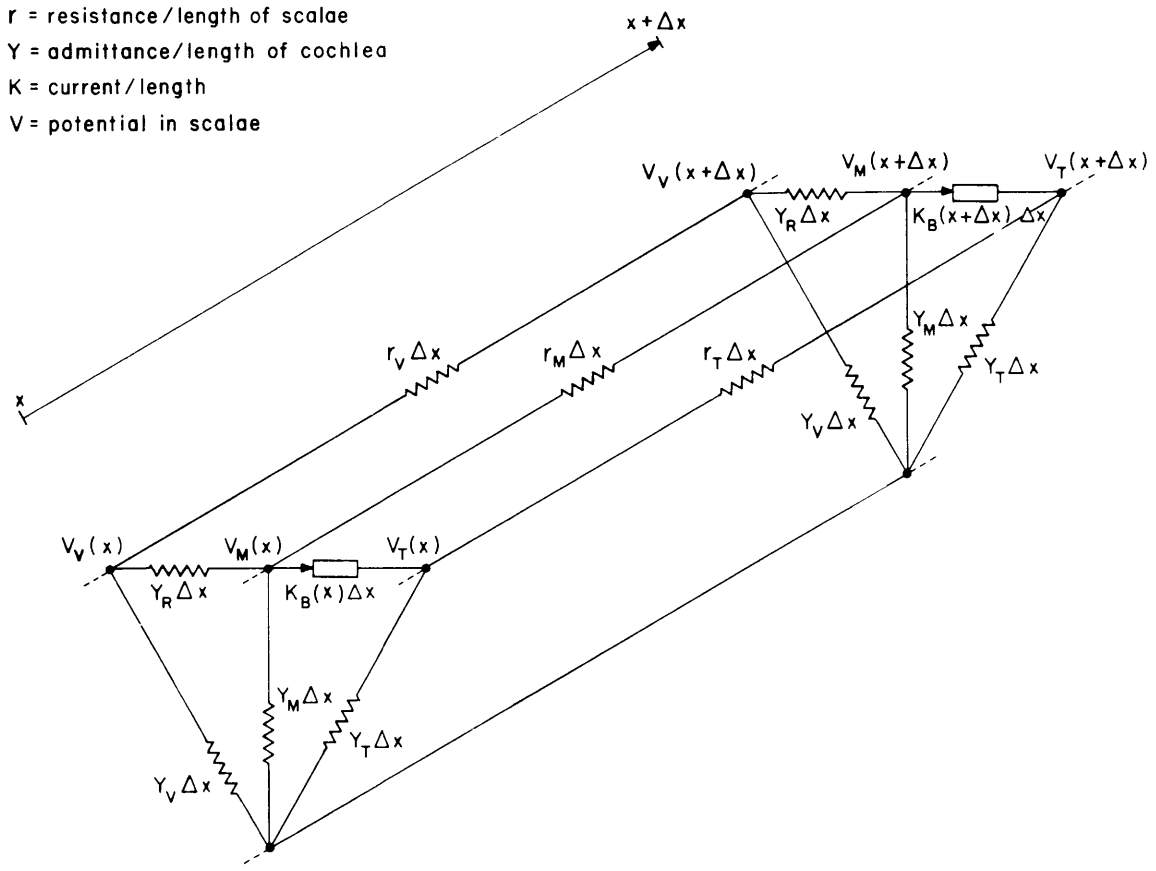

Fig. XV-28. A one-dimensional, distributed, electric network model of the cochlea. $V_V(X)$, $V_M(X)$ and $V_T(X)$ are the cochlea potentials in scalae vestibuli, media, and tympani x cm from the stapes. Y_V, Y_M and Y_T are the admittances per unit length of scala vestibuli, media, and tympani relative to ground. Y_R is the admittance per unit length across Reissner's membrane. $K_B(X)$ represents the current per unit length flowing across the organ of Corti. r_V, r_M, and r_T are the longitudinal resistances per unit length in scala vestibuli, scala media, and scala tympani.

1. If all of the admittances in the network are purely real, the ratios of potentials in any pair of scalae is independent of frequency, the phase shift of cochlear potentials across the organ of Corti is 180° independent of frequency, and the phase shift of cochlear potentials across Reissner's membrane is 0°.

2. To obtain results from such a network which are even qualitatively consistent with our data at least one of three conditions must obtain:

(a) The admittances in the network are complex; that is, the various boundaries of the cochlea scalae have admittance with significant reactive components at frequencies as low as 100 Hz.

(b) The voltage-current characteristic of the organ of Corti cannot be modelled as a two-terminal device, and presumably some current flows in the longitudinal direction in the organ of Corti.

(c) There is significant electrical coupling of cochlear potentials between different turns of the cochlea through the bony wall.

At present, data are not available to allow us to decide among these alternatives.

b. Relation of Cochlear Potentials to Stapes Velocity

The magnitude of the ratio of cochlear potential to stapes velocity is shown as a function of frequency for 7 cochleae, in Fig. XV-29. The gross electrodes were located on the surface of the cochleae. These transfer functions have been calculated from data like those in Fig. XV-22 plus corresponding curves for the sound pressure outside the tympanic membrane and an average transfer function for the middle ear of the cat.[10] The curves are all reasonably flat (±5 dB) from 100 Hz to 10 kHz. For frequencies below 100 Hz the transfer function seems to roll off somewhat. Thus the data indicate that over a wide frequency range the cochlear potential recorded on the surface of the cochlea is of the order of 1 μV for 1 μ/sec of stapes velocity.

Transfer functions for different stimulus levels obtained from one cochlea are shown in Fig. XV-30. The sequence of transfer functions for decreasing stimulus level appear to converge upward to a single curve. The upper three curves obtained at the three lowest stimulus levels show very little deviation from each other. In this respect, at least, the system generating cochlear potentials can be represented as a linear system. At the lower stimulus levels the transfer function becomes flatter and relatively independent of stimulus frequency. At the higher stimulus levels the transfer function deviates significantly from a constant and the cochlear potential is no longer proportional to the stapes velocity.

Similar data obtained from microelectrodes inserted into the cochlear scalae lead to somewhat similar conclusions although the results depend somewhat upon which scala the electrode is in. The electrical characteristics of microelectrodes limit their

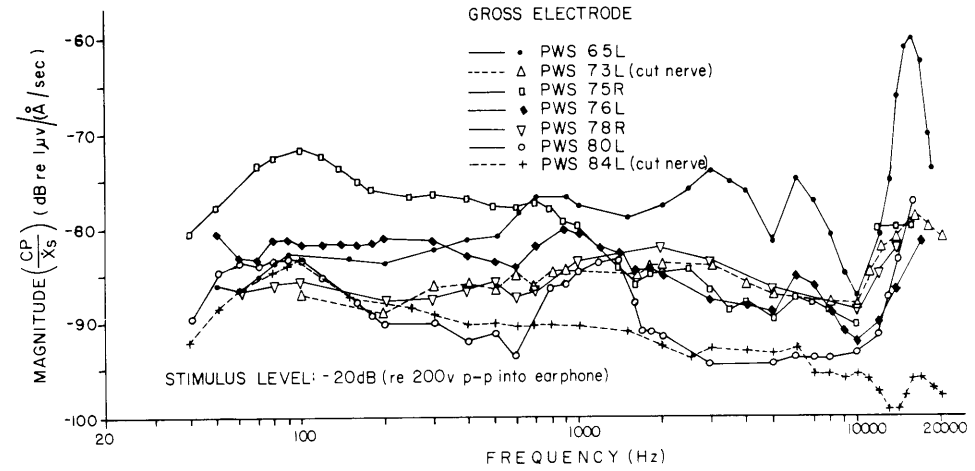

Fig. XV-29. Ratio of magnitudes of cochlear potential and stapes velocity for 7 cochleae. These data were obtained from a gross electrode on the surface of the cochlea. Solid lines correspond to data from normal cochleae. Dashed lines correspond to data from cochleae whose auditory nerve had been severed.

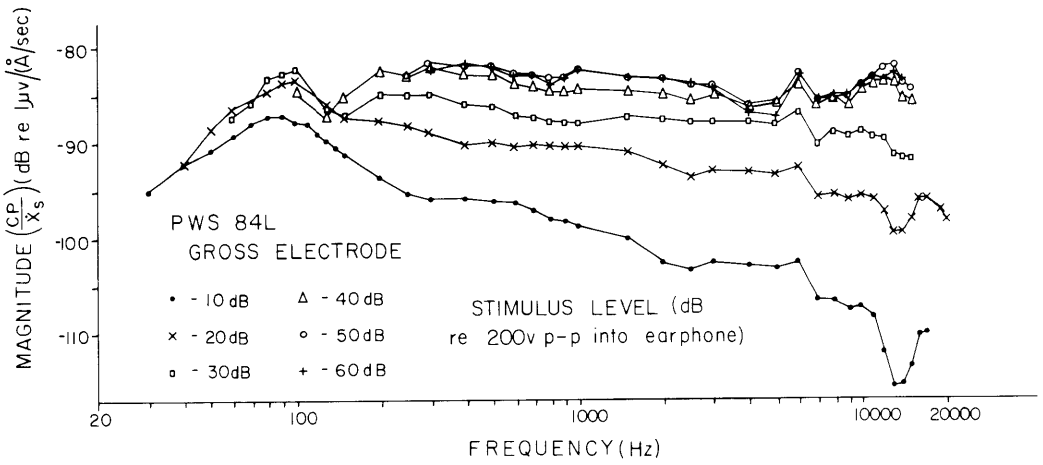

Fig. XV-30. Ratio of magnitudes of cochlear potential and stapes velocity for one cochlea. The parameter is stimulus level. These data were obtained from a gross electrode on the surface of the cochlea. The auditory nerve had been sectioned in this animal.

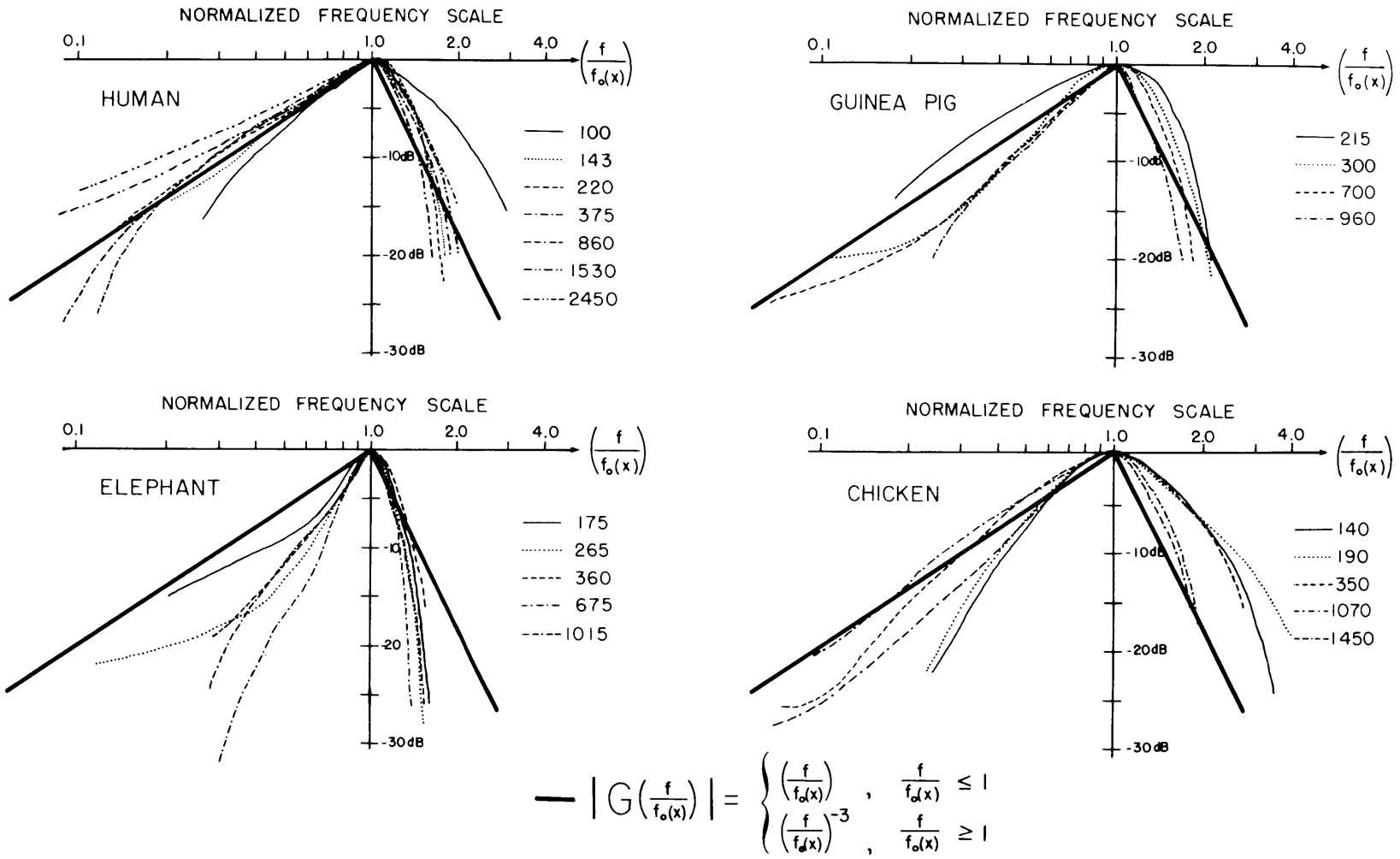

Fig. XV-31. Ratio of magnitude of cochlear partition displacement to stapes displacement as a function of frequency for 4 species. Ordinate scale is normalized and logarithmic. Abscissa is a normalized frequency scale where $f_o(x)$ is the frequency at which the response is maximum for a point x cm from the stapes. For each species, the parameter given in the legend is f_o. The heavy line is the function 20 log $|G(f/f_o(x))|$, which has a slope of +20 dB/decade for $\frac{f}{f_o(x)} \leq 1$ and -60 dB/decade for $\frac{f}{f_o(x)} \geq 1$. The data were obtained from von Békésy.[11-13]

frequency response to a few kilohertz and thus, in addition, we cannot be certain of the relation between the magnitude of the intracochlear potential and stapes velocity at higher frequencies.

The result that the magnitude of the cochlear potential is proportional to the stapes velocity over a broad frequency range is consistent with the hypothesis that cochlear potential is proportional to basilar membrane displacement. The mechanical data of von Békésy[11-13] are shown plotted in normalized, logarithmic coordinates in Fig. XV-31. The displacement of the cochlear partition for a constant stapes displacement is shown as a function of frequency for 4 species. The frequency scale is normalized to the frequency at which the maximum response was obtained for each position along the cochlea. The heavy line is a function that rises at 20 dB/decade below the corner frequency, and falls at -60 dB/decade above the corner frequency.

Since the 20 dB/decade line fits the data for frequencies below the corner frequency, the magnitude of the displacement of the cochlear partition is proportional to the magnitude of the stapes velocity. Von Békésy[14] has reported that cochlear microphonic potentials are proportional to the displacement of the cochlear partition. If we accept these two results, then it can be concluded that the magnitude of the cochlear potential is proportional to stapes velocity below the corner frequency. From Schuknecht's data[15] one can conclude that the corner frequencies are above approximately 15 kHz for points along the cochlear partition located in the most basal region of the cat's cochlea. Thus our finding that the magnitude of cochlear potential is proportional to the magnitude of the stapes velocity is consistent with the mechanical measurements (Fig. XV-31) and the mechano-electrical measurement[14] of von Békésy.

T. F. Weiss, W. T. Peake, H. S. Sohmer

References

1. H. Davis, "The Electrical Phenomena of the Cochlea and the Auditory Nerve," J. Acoust. Soc. Am. 6, 205-215 (1935).
2. I. Tasaki and C. Fernandez, "Modification of Cochlear Microphonics and Action Potentials by KCl Solution and by Direct Currents," J. Neurophysiol. 15, 497-512 (1952).
3. I. Tasaki, H. Davis, and D. H. Eldredge, "Exploration of Cochlear Potentials in Guinea Pig with a Microelectrode," J. Acoust. Soc. Am. 26, 765-773 (1954).
4. I. Tasaki, "Hearing," Ann. Rev. Physiol. 19, 417-438 (1957).
5. C. Fernandez, R. Butler, T. Konishi, V. Honrubia, and I. Tasaki, "Cochlear Potentials in the Rhesus and Squirrel Monkey," J. Acoust. Soc. Am. 34, 1411-1417 (1962).
6. T. Konishi and T. Yasuno, "Summating Potential of the Cochlea in the Guinea Pig," J. Acoust. Soc. Am. 34, 1448-1452 (1963).
7. M. Lawrence, "Dynamic Range of the Cochlear Transducer," Cold Spring Harbor Symposia on Quantitative Biology, Vol. 30, pp. 159-167, 1965.

8. M. Lawrence, "Electrical Polarization of the Tectorial Membrane," Ann. Otol. Rhinol. Laryngol. 76, 287-312 (1967).

9. T. F. Weiss, W. T. Peake, and H. S. Sohmer (unpublished).

10. J. J. Guinan and W. T. Peake, "Middle-Ear Characteristics of Anesthetized Cats," J. Acoust. Soc. Am. 41, 1237-1261 (1967).

11. G. von Békésy, Experiments in Hearing, edited by E. G. Wever (McGraw-Hill Book Company, New York, 1960), pp. 446-460.

12. Ibid., pp. 460-469.

13. Ibid., pp. 500-510.

14. Ibid., pp. 672-684.

15. H. F. Schuknecht, "Neuroanatomical Correlates of Auditory Sensitivity and Pitch Discrimination in the Cat," Neural Mechanisms of the Auditory and Vestibular Systems, G. L. Rasmussen and W. F. Windle (eds.) (Charles C. Thomas, Publisher, Chicago, Ill., 1960), pp. 76-90.

F. EFFECT OF CUTTING THE MIDDLE-EAR MUSCLES ON TRANSMISSION IN ANESTHETIZED CATS

Although it has been demonstrated many times that middle-ear muscles do not contract in barbiturate anesthetized cats,[1] in certain experiments it is desirable to section the middle-ear muscles to be absolutely sure that they are not acting on the ossicular chain. For instance, in experiments in which electrical or high-intensity acoustic stimulation is used, the precaution has become standard in our laboratory.[2,3] The question then arises whether or not middle-ear transmission is affected by the passive loading of the middle-ear muscles on the ossicular chain. The experiments reported here were designed to answer this question.

1. Methods

From a ventral approach the auditory bulla was exposed, and the bulla and bony septum opened. Cochlear potentials were recorded from gross electrodes placed on or near the round window in nine cats. A sinusoidal acoustic stimulus was swept from 20 Hz to 40,000 Hz, and the fundamental component of the cochlear potential was recorded by the method described in Fig. XV-21 (Sec. XV-E). Differences in these records were measured which resulted from the following procedures: (a) measured volumes of physiological saline (0.9% NaCl) were introduced into the middle-ear cavity, (b) the corda tympani nerve was cut, (c) the process of the malleus to which the tensor-tympani tendon attaches was cut, and (d) the stapedius tendon was sectioned.

On two cats a somewhat different method was tried in which a feedback system kept the cochlear potential amplitude constant during the sweep, and the stimulus attenuation was recorded. This method yielded approximately the same curves as the constant stimulus-voltage sweeps, thereby showing that the system was approximately linear for the levels used.

2. Results

The addition of 0.9% NaCl into the middle ear caused changes ranging from a 15-dB reduction to a 6-dB increase for fluid levels below (i.e., dorsal to) the round window. The dependence of these changes on the frequency varied considerably from one ear to another. In two cases the changes were between 0 and -2 dB throughout the frequency range. We may conclude that relatively large quantities of fluid (up to ~0.2 cm^3) in the dorsal part of the middle-ear cavity (even covering the stapes) can have relatively small effects on middle-ear transmission.

Results from cutting the middle-ear muscles can be seen in Fig. XV-32. The

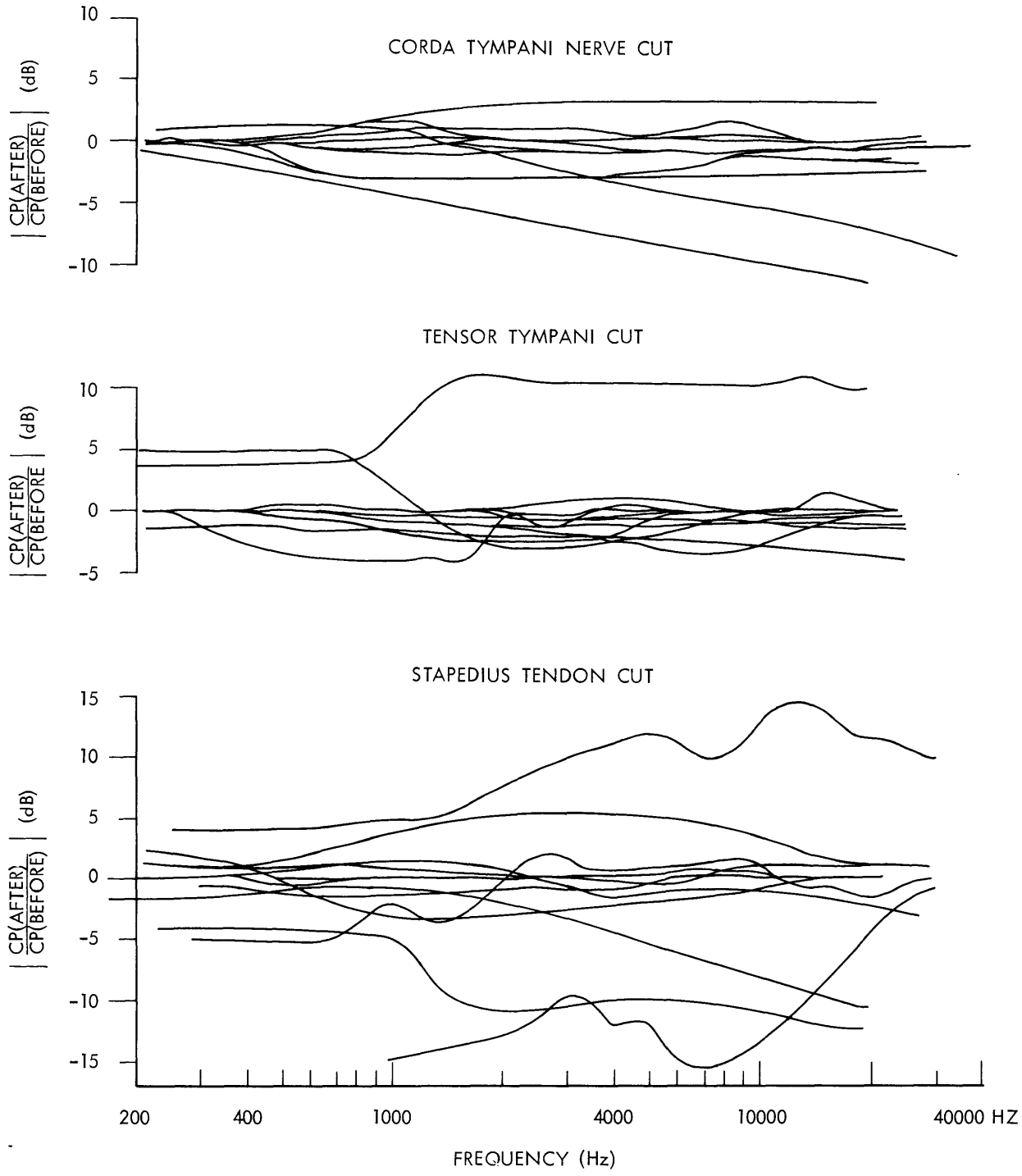

Fig. XV-32. Sequential results of cutting the corda tympani, the malleus process to the tensor tympani, and the stapedius tendon of 12, 12, and 13 ears, respectively.

variability of these measurements was due, in part, to the effect of moisture in the wick electrode, which was used in most cases. With too much moisture the round window was flooded, and with too little the electrode would dry out. Both occurrences resulted in attenuated cochlear potentials, and hence the records often showed considerable variability. In order to observe the stapedius tendon before it was sectioned, the styloid projection had to be pushed out of the way or removed. This procedure required more time than the others, and probably contributes to the larger variability among ears in the third graph.

We may conclude from the results shown in Fig. XV-32 that detaching the middle-ear muscles from the ossicles can have a relatively small effect on the transmission of the middle ear. Hence the average transfer function for the middle ear of anesthetized cats, which was obtained with the muscles intact,[1] is applicable to data obtained with the muscles cut.

A. D. Drake, W. T. Peake

References

1. J. J. Guinan, Jr. and W. T. Peake, "Middle-Ear Characteristics of Anesthetized Cats," J. Acoust. Soc. Am. 41, 1237-1261 (1967).
2. M. L. Wiederhold, "A Study of Efferent Inhibition of Auditory Nerve Activity," Ph. D. Thesis, Department of Electrical Engineering, M. I. T., 1967.
3. N. Y. S. Kiang, T. Baer, E. M. Marr, and D. Demont, "Discharge Rates of Single Auditory-Nerve Fibers as Functions of Tone Level," J. Acoust. Soc. Am. (in press).